The 12th Symposium on Polar Science
15 – 18 November 2021

National Institute of Polar Research
Research Organization of Information and Systems

Session OG
Polar Geosciences

Program and Abstracts

Convener : Jun'ichi OKUNO (NIPR)

【OG】Polar Geosciences

Scopes

This session covers research topics from the fields of geology, mineralogy, geomorphology, quaternary research, geodesy, and solid Earth geophysics.

Convener : **Jun'ichi OKUNO (NIPR)**

Real-time Oral and poster presentations (10:30 – 12:10, 13:30 - 14:50, 15:30-)

Date: Mon. 15 November

Chair: Mami Takehara (NIPR)(9:55～ Announcement)				
OGo1	10:30 - 10:50	Current understanding of the geologic framework of easternmost part of Dronning Maud Land and western part of Enderby Land, and future plan (JARE 65-)	*Tomokazu Hokada (NIPR), JARE geology group	OGo01_Hokada_00058_03.pdf
OGo2	10:50 - 11:10	U-Pb zircon geochronology of high-grade metamorphic rocks from outcrops along the Prince Olav Coast, East Antarctica	*Ippei Kitano (Tochigi Prefectural Museum), Tomokazu Hokada (NIPR), Sotaro Baba (University of the Ryukyus), Atsushi Kamei (Shimane University), Yoichi Motoyoshi (NIPR), Tsuyoshi Toyoshima (Niigata University), Masahiro Ishikawa (Yokohama National University), Takuma Katori (Fossa Magna Museum), Nobuhiko Nakano (Kyushu University), Yasuhito Osanai (Kyushu University)	OGo02_Kitano_00505_01.pdf
OGo3	11:10 - 11:30	Long-lived anatexis in Rundvagshetta, Lützow-Holm Complex, East Antarctica	*Kota Suzuki (Kyoto University),Tetsuo Kawakami (Kyoto University), Shuhei Sakata (ERI, University of Tokyo)	OGo03_Suzuki_00515_01.pdf
OGo4	11:30 - 11:50	Pressure-Temperature path of a garnet-biotite-sillimanite gneiss from the Oyayubi ridge, Brattnipene, Sør Rondane Mountains.	*Tatsuro Adachi (Kyushu University),Tetsuo Kawakami (Kyoto University), Masaoki Uno (Tohoku University), Fumiko Higashino (Kyoto University)	OGo04_Adachi_00047_01.pdf
OGo5	11:50 - 12:10	Highlights of the Student Himalayan Exercise Tour 9 years and invitation to the 10th tour	*Masaru Yoshida (Gondwana Institute for Geology and Environment, Tribhuvan University), Student Himalayan Field Exercise Project	OGo05_Yoshida_00487_01.pdf
	12:10 - 13:20	Break		
Chair: Takeshige Ishiwa (NIPR)(13:25～ Announcement)				
OGo6	13:30 - 13:50	Paleostress inversion in hydro-fractured metamorphic complex using 3D aerophotography images (Sør Rondane Mountains, East Antarctica)	*Masaoki Uno (Tohoku University), Tetsuo Kawakami (Kyoto University), Tatsuro Adachi (Kyushu University), Fumiko Higashino (Kyoto University)	OGo06_Uno_00116_01.pdf
OGo7	13:50- 14:10	Estimation of Shirase Glacier flow velocity from 2018 to 2021 using Sentinel-1 data	*Shotaro Ohkawa (The Graduate University for Advanced Studies), Koichiro Doi (NIPR), Kazuki Nakamura (Nihon University), Hiroto Nagai (Waseda University)	OGo07_Ohkawa_00614_01.pdf
OGo8	14:10 - 14:30	Episodes of West Antarctic Ice Sheet retreat during Pliocene warmth revealed by a sedimentary record from the Amundsen Sea	*Keiji Horikawa (University of Toyama), Masahiro Noda (University of Toyama), Miyu Fujimoto (University of Toyama), Yoshihiro Asahara (Nagoya University), Ki-Cheol Shin (Research Institute for Humanity and Nature), Masao Iwai (Kochi University), Li Wu (Tongji University), Ellen Cowan (Appalachian State University), Christine Siddoway (Colorado College), Claus-Dieter Hillenbrand (British Antarctic Survey)	OGo08_Horikawa_00521_01.pdf
OGo9	14:30 - 14:50	Sea-level changes in East Antarctica based on glacial isostatic adjustmet modeling since the Last Interglacial period	*Takeshige Ishiwa (NIPR), Jun'ichi Okuno (NIPR), Yusuke Suganuma (NIPR)	OGo09_Ishiwa_00105_01.pdf
	15:00 - 15:30	Break		
Chair: Jun'ichi Okuno (NIPR)				
	15:30 - 16:00	Poster session core time		
	16:00 - 17:30	Free discussion in each presenter's room (oral and poster presenters)		

Poster presentations (15 November - 18 December)

OGp01	Barberton impact spherules, South Africa: pursuing of shock metamorphism by using Raman spectroscopy	*Arpad Csamer (University of Debrecen), Diana Skita (University of Debrecen), Istvan Rigo (Wigner Research Centre for Physics), Miklos Veres (Wigner Research Centre for Physics), Peter Futo (University of Debrecen), Jozsef Vanyo (Eszterhazy Karoly University), Arnold Gucsik (Eszterhazy Karoly University)	OGp01_Csamer_00558_01.pdf

OGp02	Absolute Gravity Measurements Planned in JARE63	*Koichiro Doi (NIPR), Akito Araya (ERI, The University of Tokyo), Daisuke Oka (Hokkaido Research Organization), Yoichi Fukuda (NIPR), Yuichi Aoyama (NIPR), Jun'ichi Okuno (NIPR), Akihisa Hattori (SOKENDAI)	OGp02_Doi_00460_01.pdf
OGp03	Geochronological and petrogenesis of charnockite from Mt. Cronus, Napier Complex, Enderby Land, East Antarctica	*Miku Endo (Yamagata University), Kenichiro Tani (National Museum of Nature and Science), Shin-ichi Kagashima (Yamagata University)	OGp03_Endo_00492_01.pdf
OGp04	Unveiling seafloor spreading mode and geodynamics in the Southeast Indian Ridge: New challenge in Japanese Antarctic Research Expedition	*Masakazu Fujii (NIPR)	OGp04_Fujii_00252_01.pdf
OGp05	Counterclockwise and clockwise P-T histories recorded in a single sample? (Brattnipene, Sør Rondane Mountains, East Antarctica)	*Hayato,Ikeda (Kyoto University), Tetsuo Kawakami (Kyoto University), Higashino Fumiko (Kyoto University)	OGp05_Ikeda_00361_01.pdf
OGp06	Monazite U-Th-Pb ages of the "unnamed nunatak (Nunatak 170224-3)" east of Forfinger Point, Western Rayner Complex, Enderby Land, East Antarctica	*Tomokazu Hokada (NIPR), Sotaro Baba (University of the Ryukyus), Atsushi Kamei (Shimane University), Ippei Kitano (Kyushu University)	OGp06_Hokada_00058_02.pdf
OGp07	Preliminary reports of U-Pb zircon age of charnockites in Aker Peaks of the Napier Complex, East Antarctic	*Kenji Horie (NIPR), Mami Takehara (NIPR), Tomokazu Hokada (NIPR), Allen Nutman (University of Wollongong)	OGp07_Horie_00613_01.pdf
OGp08	Dependence of GIA-induced gravity change in Antarctica on viscoelastic Earth structure	*Yoshiya Irie (NIPR), Jun'ichi Okuno (NIPR), Takeshige Ishiwa (NIPR), Koichiro Doi (NIPR), Yoichi Fukuda (NIPR)	OGp08_Irie_00219_01.pdf
OGp09	Monitoring and assessing the permafrost coast retreat along the Kara Sea by integrating in situ measurements	*Arata Kioka (Kyushu University), Vladislav Isaev (Lomonosov Moscow State University), Pavel Kovov (Lomonosov Moscow State University), Takeshi Tsuji (Kyushu University), Stanislav Ogorodov (Lomonosov Moscow State University), Masakazu Fujii (NIPR), Osip Kokin (Lomonosov Moscow State University), Michail Tsarapov (Lomonosov Moscow State University), Andrey Koshurnikov (Lomonosov Moscow State University), Yaroslav Shevchuk (Lomonosov Moscow State University)	OGp09_Kioka_00139_01.pdf
OGp10	Metamorphic zone mapping of the High Himalayan Crystalline nappe in Dhankuta, Eastern Nepal	*Shumpei Kudo (Kyoto University), Tetsuo Kawakami (Kyoto University), Nakajima Toru (Tono Geoscience Center), Harutaka Sakai (Kyoto University)	OGp10_Kudo_00588_02.pdf
OGp11	Characteristics and evolution process of tectonic regions in the Antarctic Plate and its adjacent area based on marine geophysical data	*Takeshi Matsumoto (University of the Ryukyus), Yoshifumi Nogi (NIPR)	OGp11_Matsumoto_00154_01.pdf
OGp12	Dependence of the Holocene rapid melting on GIA-induced vertical rate in East Antarctica	*Jun'ichi Okuno (NIPR), Akihisa Hattori (SOKENDAI), Yoshiya Irie (NIPR), Yuichi Aoyama (NIPR), Koichiro Doi (NIPR), Yoichi Fukuda (NIPR)	OGp12_Okuno_00050_01.pdf
OGp13	Ice sheet thinning since the Last Glacial Maximum in central Dronning Maud Land, East Antarctica	*Yusuke Suganuma (NIPR), Heitaro Kaneda (Chuo University), Takushi Koyama (Oita University), Takeshige Ishiwa (NIPR), Jun'ichi Okuno (NIPR), Motohiro Hirabayashi (NIPR)	OGp13_Suganuma_00126_01.pdf
OGp14	Geochemical characterization of zircons for age determination of metamorphism in Fyfe Hills of the Napier Complex, East Antarctica	*Mami Takehara (NIPR), Kenji Horie (NIPR), Tomokazu Hokada (NIPR)	OGp14_Takehara_00345_01.pdf
OGp15	Ancient earthquakes and E-W compressional stress field recorded by brittle faults and pseudotachylytes from southwestern Skarvsnes in the Lützow-Holm Complex, East Antarctica	*Tsuyoshi Toyoshima (Niigata University), Ippei Kitano (Tochigi Prefectural Museum), Masahiro Ishikawa (Yokohama National University), Takuma Katori (Fossa Magna Museum), Tomokazu Hokada (NIPR)	OGp15_Toyoshima_00267_01.pdf
OGp16	C-O-H fluid was present during the garnet-forming partial melting in the Aoyama area, Ryoke metamorphic belt, SW Japan	*Natsumi Yoshimoyo (Kyoto University), Tetsuo Kawakami (Kyoto University)	OGp16_Yoshimoto_00527_01.pdf

Current understanding of the geologic framework of easternmost part of Dronning Maud Land and western part of Enderby Land, and future plan (JARE 65-)

Tomokazu Hokada[1,2], and JARE geology group
[1] *National Institute of Polar Research*
[2] *Department of Polar Science, The Graduate University for Advanced Studies (SOKENDAI)*

The JARE's basement geology programs have covered the area of longitude between 10°E and 55°E of the Antarctic continent, and published total 39 sheets of geological map series. This part of the Antarctic continent comprises of deep crustal high-grade metamorphic and plutonic rocks that recorded the geologic history over 3 billion years, and is, therefore, ideal field for investigating long Earth history and deep crustal processes. Following the temporal geologic summary by Shiraishi et al. (2008), significant scientific advance has been made for the basement geology especially of easternmost part of Dronnning Maud Land and western part of Enderby Land regions by JARE geology group, such as numerous numbers of zircon ages published so far for the Lützow-Holm Complex (e.g., Dunkley et al., 2020; and references therein) and for western Enderby Land (e.g., Horie et al., 2012, 2016; Hokada et al., poster presentation of this symposium). Not only of age constraints, geological and petrological information for these regions have been accumulated. This presentation summarizes the current understanding of the geologic flame work of this part of Antarctica, and proposes the future geologic field plan at next phase of JARE program (phase-X; JARE 65-).

References

Dunkley, D.J., Hokada, T., Shiraishi, K., Hiroi, Y., Nogi, Y., Motoyoshi, Y., Geological subdivision of the Lützow–Holm Complex in East Antarctica: from the Neoarchean to the Neoproterozoic. Polar Science, 26, 100606, 2020.

Horie, K., Hokada, T., Motoyoshi, Y., Shiraishi, K., Hiroi, Y., Takehara, M., U-Pb zircon geochronology in the western part of the Rayner Complex, East Antarctica. Journal of Mineralogical and Petrological Sciences, 111, 104-117, 2016.

Shiraishi, K., Dunkley, D.J., Hokada, T., Fanning, C.M., Kagami, H., Hamamoto, T., Geochronological constraints on the Late Proterozoic to Cambrian crustal evolution of eastern Dronning Maud Land, East Antarctica: a synthesis of SHRIMP U-Pb age and Nd model age data. In: Satish-Kumar, M. et al. (Eds.), Geodynamic Evolution of East Antarctica: A Key to the East-West Gondwana Connection. Geological Society, London, Special Publication, 308, 21-67, 2008.

U–Pb zircon geochronology of high-grade metamorphic rocks from outcrops along the Prince Olav Coast, East Antarctica

Ippei Kitano[1,2], Tomokazu Hokada[3,4], Sotaro Baba[5], Atsushi Kamei[6], Yoichi Motoyoshi[3,4], Tsuyoshi Toyoshima[7], Masahiro Ishikawa[8], Takuma Katori[7,9], Nobuhiko Nakano[1], and Yasuhito Osanai[1]

[1] *Kyushu University*

[2] *Tochigi Prefectural Museum*

[3] *National Institute of Polar Research*

[4] *Department of Polar Science, The Graduate University for Advanvced Studies (SOKENDAI)*

[5] *University of the Ryukyus*

[6] *Shimane University*

[7] *Niigata University*

[8] *Yokohama National University*

[9] *Fossa Magna Museum*

The Lützow-Holm Complex (LHC) is composed of high-grade metamorphic rocks and associated intrusive rocks sporadically exposing along the Prince Olav Coast and around the Lützow-Holm Bay, East Antarctica (e.g., Shiraishi et al., 1994). The LHC is characterized by the southwestward increase in metamorphic grade from amphibolite- to granulite-facies and high- to ultrahigh-temperature metamorphic conditions during *ca.* 650–500 Ma (e.g., Hiroi et al., 1983; Shiraishi et al., 1994; Motoyoshi and Ishikawa, 1997; Hokada and Motoyoshi, 2006; Yoshimura et al., 2008; Kawasaki et al., 2011; Dunkley et al., 2014; Tsunogae et al., 2015; Takamura et al., 2018, 2020), except for the early Neoproterozoic metamorphic rocks in the Cape Hinode within the LHC (Dunkley et al., 2014). Dunkley et al. (2020) have divided the lithology into 6 suites of the Innhovde Suite (protolith ages of orthogneisses: 1070–1040 Ma), Rundvågshetta Suite (protolith ages of orthogneisses: 2520–2470 Ma), Skallevikshalsen Suite (protolith ages of orthogneisses: 1830–1790 Ma), Langhovde Suite (protolith ages of orthogneisses: 1100–1050 Ma), East Ongul Suite (protolith ages of orthogneisses: 630 Ma), and Akarui Suite (protolith ages of orthogneisses: 970–800 Ma) with the exotic block of Hinode Block metamorphosed at *ca.* 970–960 Ma, by compiling the U–Pb age dataset accumulated within recent two decades. However, the blank areas for the U–Pb zircon dating still remain in the LHC, leading the interruption to understand its comprehensive thermal history. Recently, another thermal event at *ca.* 930 Ma in the LHC was reported by Baba et al. (2021) from garnet–biotite gneiss in the Akebono Rock. This study will provide the results of zircon U–Pb dating from high-grade metamorphic rocks in 8 outcrops (Sinnan Rocks, Akebono Rock, Niban Rock, Gobanme Rock, Tenmondai Rock, Akarui Point, Cape Omega and Oku-iwa Rock) along the Prince Olav Coast (Fig. 1). These outcrops were investigated through the operations of the 58th and 60th Japanese Antarctica Research Expeditions, and belong to the Akarui Suite of Dunkley et al. (2020).

The dating results in this study is summarized in Table 1. The trace of *ca.* 1000 Ma metamorphism was newly detected from garnet–sillimanite–biotite gneiss in the Niban Rock. The metamorphic age of *ca.* 930 Ma was also confirmed from staurolite-bearing garnet–gedrite–biotite–chlorite gneiss in the Akebono Rock. The metamorphic zircons in other analyzed samples showed late Neoproterozoic ages of >600–500 Ma. The relic detrital domains of zircons in analyzed paragneisses were characterized by late to middle Neoproterozoic ages with/without minor Archean to early Neoproterozoic ages.

Based on the results of this study, Baba et al. (2021), and Dunkley et al. (2020), it indicates the multi-thermal events at *ca.* 1000–960 Ma, 930 Ma, and >600–500 Ma in the LHC along the Prince Olav Coast. The metamorphic rocks in the Cape Hinode and Niban Rock record the earliest metamorphism and detrital sources of *ca.* 3300–1000 Ma and 1940–1040 Ma for their sedimentary protoliths, respectively. According to Dunkley et al. (2014), the Niban Rock was reworked by later magmatism at *ca.*

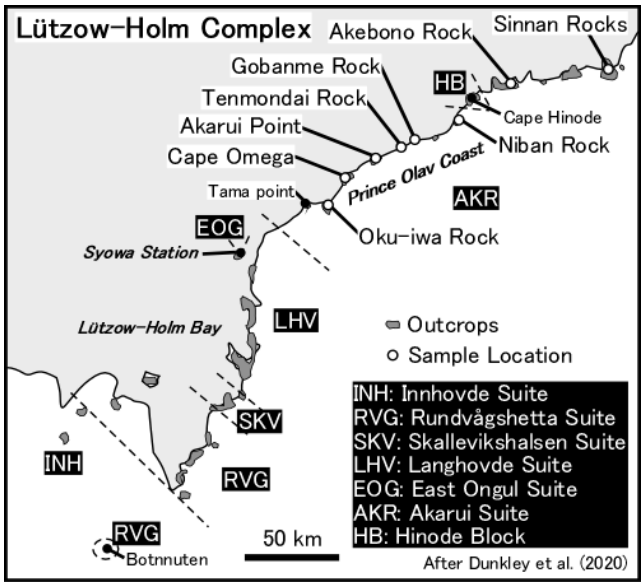

Figure 1. The lithological division in the Lützow-Holm Complex after Dunkley et al. (2020) and sample locations.

940 Ma and 550 Ma. The Akebono Rock is the sole outcrop in the LHC to possess the thermal history at *ca.* 930 Ma without younger overprinting as well as unique paragneisses featured by the detrital zircon ages narrowly ranging from *ca.* 1120 Ma to 1010 Ma. The other outcrops of Sinnan Rocks, Gobanme Rock, Tenmondai Rock, Akarui Point, Cape Omega, Oku-iwa Rock and Tama Point along the Prince Olav Coast underwent the extensive high-grade metamorphism during *ca.* 650–500 Ma. The presence of *ca.* 1200–700 Ma detrital zircons characterizes the paragneisses in these areas except for Oku-iwa Rock and Tama Point where no paragneisses occur. Therefore, these characteristics of zircon U–Pb chronology suggests the LHC along the Prince Olav Coast is likely a collage of three distinct segments which originated from different detritus provenances and metamorphosed at *ca.* 1000–960 Ma, 930 Ma, and 650–500 Ma, respectively.

Table 1. The summary of results of zircon U–Pb dating in this study.

Sample No.	location	Rock type	Zircon U-Pb ages (Ma)		
			Metamorphic domain	Detrital domain	Inherited domain
IK16123001A	Sinnan Rocks	Crn-Sil-Bt-Ms gneiss	640-490		
IK16123003A	Sinnan Rocks	Grt-bearing Bt gneiss	660-510	890	
IK16123102	Akebono Rock	St-bearing Grt-Ged-Bt-Chl gneiss	934 ± 11		
IK19011606A	Niban Rock	Grt-Sil-Bt gneiss	998.0 ± 9.7	1940-1760, 1300, 1160-1040	
IK19011805A	Gobanme Rock	Grt-Sil-Bt gneiss	630-530	1860-1710, 1050-930	
IK17011002A	Tenmondai Rock	Grt-Spl-Sil-Bt gneiss	620-530	3330, 2400, 2090-1730, 1080-800	
IK17010601	Akarui Point	Grt-Bt gneiss	620-500		
IK17010904A	Cape Omega	Sil-bearing Grt-Bt gneiss	630-520	1030-860	
IK19011404A	Oku-iwa Rock	Grt-Opx granulite	610-480		1020~

References

Baba, S., Horie, K., Hokada, T., Takehara, M., Kamei, A., Kitano, I. and Motoyoshi, Y., U-Pb zircon age of Grt-Bt gneiss in Akebono Rock, Prince Olav Coast, East Antarctica. The 128th Annual Meeting of the Geological Society of Japan, Abstract, 2021.

Dunkley, D.J., Shiraishi, K., Motoyoshi, Y., Tsunogae, T., Miyamoto, T., Hiroi, Y. and Carson, C., Deconstructing the Lützow-Holm Complex with zircon geochronology. 7th International SHRIMP Workshop, Abstract, 2014.

Dunkley, D.J., Hokada, T., Shiraishi, K., Hiroi, Y., Nogi, Y. and Motoyoshi, Y., Geological subdivision of the Lützow–Holm Complex in East Antarctica: From the Neoarchean to the Neoproterozoic. Polar Science, 26, 100606, 2020.

Hiroi, Y., Shraishi, K., Yanai, K. and Kizaki, K., Aluminum slicates in the Prince Olav and Sôya Coasts, East Antarctica. Memoirs of National Institute of Polar Research. Special issue, 28, 115-131, 1983.

Hokada, T. and Motoyoshi, Y., Electron microprobe technique for U–Th–Pb and REE chemistry of monazite, and its implications for pre-, peak- and post-metamorphic events of the Lützow-Holm Complex and the Napier Complex, East Antarctica. Polar Geoscience, 19, 118-151, 2006.

Kawasaki, T., Nakano, N. and Osanai, Y., Osumilite and a spinel + quartz association in garnet-sillimanite gneiss from Rundvågshetta, Lützow-Holm Complex, East Antarctica. Gondwana Research, 19, 430-445, 2011.

Motoyoshi, Y. and Ishikawa, M., Metamorphic and structural evolution on granulites from Rundvågshetta, Lützow-Holm Bay, East Antarctica. In: Ricci, C. L. (ed.) The Antarctic Region: Geological Evolution and Processes. Terra Antartica, Sienna, 65-72, 1997.

Shiraishi, K., Ellis, D.J., Hiroi, Y., Fanning, C.M., Motoyoshi, Y. and Nakai, Y., Cambrian orogenic belt in East Antarctica and Sri Lanka: implication for Gondwana assembly. Journal of Geology, 102, 47-65, 1994.

Takamura, Y., Tsunogae, T., Santosh, M., and Tsutsumi, Y., Detrital zircon geochronology of the Lützow-Holm Complex, East Antarctica: Implications for AntarcticaeSri Lanka correlation. Geoscience Frontiers, 9, 355-375, 2018.

Takamura, Y., Tsunogae, T., and Tsutsumi, Y., U–Pb geochronology and REE geochemistry of zircons in mafic granulites from the Lützow-Holm complex, East Antarctica: Implications for the timing and *P–T* path of post-peak exhumation and Antarctica–Sri Lanka correlation. Precambrian Research, 348, 105850, 2020.

Tsunogae, T., Yang, Q.Y. and Santosh, M., Early Neoproterozoic arc magmatism in the Lützow-Holm Complex,East Antarctica: Petrology, geochemistry, zircon U–Pb geochronologyand Lu–Hf isotopes and tectonic implications. Precambrian Research, 266, 467-489, 2015.

Yoshimura, Y., Motoyoshi, Y. and Miyamoto, T., Sapphirine+quartz association in garnet: implication for ultrahigh-temperature metamorphism at Rundvågshetta, Lützow-Holm Complex, East Antarctica. In: Satish-Kumar, M. et al. (eds.) Geodynamic Evolution of East Antarctica: A Key to the East-West Gondwana Connection. Geological Society Special Publication, 308, 377-390, 2008.

Long-lived anatexis in Rundvågshetta, Lützow-Holm Complex, East Antarctica

Kota Suzuki[1], Tetsuo Kawakami[1], and Shuhei Sakata[2]
[1]*Department of Geology and Mineralogy, Graduate School of Science, Kyoto University, Kyoto 606-8502, Japan*
[2]*Earthquake Research Institute, University of Tokyo, 1-1-1 Yayoi, Bunkyo-ku, Tokyo 113-0032, Japan*

The duration of anatexis in high-grade metamorphism is essential to understand the crustal melting processes [e.g., 1] and the tectonic settings [e.g., 2]. In the case of Rundvågshetta, Lützow-Holm Complex (LHC), East Antarctica, the linkage between the U-Pb zircon ages and the metamorphic pressure-temperature (*P-T*) evolution is still unclear, although a wide range of metamorphic zircon ages have been reported [3 and references therein]. Only the melt crystallization age of ca. 520 Ma is constrained [4]. Therefore, in this study, we aim to constrain the duration of anatexis by linking U-Pb zircon ages to a clockwise *P-T* evolution of an ultrahigh-temperature (UHT) granulite sample (TK2003010309) from Rundvågshetta.

The clockwise *P-T* evolution was constrained based on the detailed petrography of inclusion minerals in garnet [5]. Garnet in the studied UHT granulite commonly consists of the P-poor core, the P-rich mantle, and the P-poor rim. [5] interpreted that the P-poor core was formed as a peritectic product of biotite dehydration melting reaction in the prograde stage. [5] further interpreted that the P-rich mantle and the P-poor rim were formed in the peak UHT and the retrograde stages, respectively.

Zircon grains in the rock matrix commonly show four microstructural domains; (I) oscillatory-zoned core, (II) dark-CL annulus, (III) slightly bright-CL inner rim, and (IV) bright-CL outer rim. The inner rim is, however, relatively rare and it was too thin for the LA-ICP-MS U-Pb zircon dating with 20 μm spot size.

The oscillatory-zoned cores are inherited domains from the protolith that is evident from the U-Pb zircon dating giving various old ages. Regardless of the variety of detrital ages, the inherited cores are always truncated by the dark-annulus with low Th/U ratios below 0.04. The dark-annulus yielded concordia age of 562.2 ± 6.3 Ma (n = 5; 2σ error, MSWD = 1.3) and commonly includes muscovite, quartz, biotite, and melt inclusions. Therefore, we consider that the dark annulus was formed in the presence of anatectic melt during the Neoproterozoic-Cambrian high-grade metamorphism widely observed in the LHC [3 and references therein]. Although older age population zircon (ca. 620-580 Ma) is reported from quartzite in Rundvågshetta [6 and 7], no evidence for polymetamorphism was detected at least in the studied sample.

The dark-annulus is further truncated by the outer rim with higher Th/U ratios (0.08-1.13). Concordant $^{206}Pb/^{238}U$ ages of the outer rim show continuous variation from 558.3 ± 20.7 Ma to 503.7 ± 14.6 Ma and the weighted mean age was calculated to be 530.8 ± 8.2 Ma (n = 16; 2σ error, MSWD = 3.1). However, the dispersed Th/U ratios and the large MSWD may suggest that zircon grew in various timings after the formation of the dark-annulus. Sillimanite, rutile, and K-feldspar are commonly included in the outer rim.

Zircon grains are also present as inclusions in the P-poor core, the P-rich mantle, and the P-poor rim of garnet. The microstructure of inclusion zircon vary systematically with the phosphorus zoning of the host garnet. Inclusion zircon in the P-poor rim of garnet commonly show four microstructural domains that are common to the matrix zircon. However, inclusion zircon in the P-poor core of garnet always lacks the inner rim and the outer rim. Similarly, inclusion zircon in the P-rich mantle of garnet lacks the outer rim. These systematic microstructure of inclusion zircon suggests that the dark-annulus, the inner rim, and the outer rim of zircon were formed prior to or simultaneously with the P-poor core, the P-rich mantle, and the P-poor rim of garnet, respectively.

In order to further constrain the relative growth timings of the zircon and garnet domains, we used partitioning of rare earth elements (REE) between zircon and garnet [e.g., 8]. The dark-annulus showed steeply sloping HREE patterns, while the outer rim showed negatively sloping patterns. In the case of garnet, the P-poor core, the P-rich mante, and the P-poor rim showed positive, flat, and negative patterns, respectively. As a result, only the P-poor rim of garnet and some of the outer rim of zircon pair gave equilibrium REE distribution pattern [9]. Therefore, it is revealed that the dark-annulus grew prior to the growth of garnet and that the outer rim of zircon grew in various timings after the formation of the dark-annulus.

In this study, we also analyzed Ti content of zircon simultaneously with the U-Pb dating by using the method of [10]. Applying the Ti-in-zircon geothermometer [11] to the dark-annulus yielded ~750 ºC, which is ~150 ºC lower than the result of Zr-in-rutile geothermometer [12] applied to inclusion rutile in the P-poor core of garnet [5]. Because inclusion rutile is not found in the dark-annulus yet, the estimated temperature of ~750 ºC represents the minimum condition [e.g., 13]. However, inclusion minerals suggest the possible occurrence of muscovite dehydration melting during the growth of the dark-annulus and the estimated temperature of ~750 ºC is consistent with the divariant field in which the muscovite dehydration melting

reaction can occur [e.g., 14]. Therefore, the dark-annulus of zircon enabled us to deduce the prograde information of the UHT metamorphism that is not recorded in garnet.

This study revealed that anatexis had already begun at ca. 560 Ma. Taking the melt crystallization age of ca. 520 Ma into account [4], the duration of anatexis in Rundvågshetta was constrained to be at least ~40 Myr. Further U-Pb dating of the thin inner-rim of zircon may reveal the duration of the UHT itself precisely.

References

[1] Rubatto, D., Chakraborty, S., and Dasgupta, S., Timescales of crustal melting in the Higher Himalayan Crystallines (Sikkim, Eastern Himalaya) inferred from trace element-constrained monazite and zircon chronology. Contributions to Mineralogy and Petrology, 165, 349-372, 2013

[2] Harley, S.L., A matter of time: The importance of the duration of UHT metamorphism. Journal of Mineralogical and Petrological Sciences, 111, 50-72, 2016

[3] Dunkley, D.J., Hokada, T., Shiraishi, K., Hiroi, Y., Nogi, Y., and Motoyoshi, Y., Geological subdivision of the Lützow-Holm Complex in East Antarctica: From the Neoarchean to the Neoproterozoic. Polar Science, 26, 100606, 2020

[4] Fraser, G. McDougall, I. Ellis, D.J., and Williams, I.S., Timing and rate of isothermal decompression in Pan-African granulites from Rundvågshetta, East Antarctica. Journal of Metamorphic Geology, 18, 441-454, 2000

[5] Suzuki, K., and Kawakami, T, Pressure-temperature-melting history of ultrahigh-temperature metamorphic rock constrained by Zr-in-rutile geothermometer: an example from Rundvågshetta in the Lützow-Holm Complex of East Antarctica. The Abstracts 2020 Online Annual Meeting of Japan Association of Mineralogical Sciences, 2020

[6] Dunkley, D.J., Shiraishi, K., Motoyoshi, Y., Tsunogae, T., Miyamoto, T., Hiroi, Y., and Carson, C.J., Deconstructing the Lützow-Holm Complex with Zircon Geochronology. Extended Abstract of 7th International SHRIMP Workshop, 116-121, 2014

[7] Takamura, Y., Tsunogae, T., Santosh, M., and Tsutsumi, Y., Detrital zircon geochronology of the Lützow-Holm Complex, East Antarctica: Implications for Antarctica-Sri Lanka correlation. Geoscience Frontiers, 9, 355-375, 2018

[8] Kawakami, T., Horie, K., Hokada, T., Hattori, K., and Hirata, T., Disequilibrium REE compositions of garnet and zircon in migmatites reflecting different growth timings during single metamorphism (Aoyama area, Ryoke belt, Japan). Lithos, 338-339, 189-203, 2019

[9] Taylor, R.J.M., Harley, S.L., Hinton, R.W., Elphick, S., Clark, C., and Kelly, N.M., Experimental determination of REE partition coefficients between zircon, garnet and melt: A key to understanding high-*T* crustal processes. Journal of Metamorphic Geology, 33, 231-248, 2015

[10] Yuguchi, T., Ishibashi, K., Sakata, S., Yokoyama, T., Itoh, D., Ogita, Y., Yagi, K., and Ohno, T., Simultaneous determination of zircon U-Pb age and titanium concentration using LA-ICP-MS for crystallization age and temperature. Lithos, 372-373, 105682, 2020

[11] Ferry, J.M., and Watson, E.B., New thermodynamic models and revised calibrations for the Ti-in-zircon and Zr-in-rutile thermometers. Contributions to Mineralogy and Petrology, 154, 429-437, 2007

[12] Tomkins, H.S., Powell, R., and Ellis, D.J., The pressure dependence of the zirconium-in-rutile thermometer. Journal of Metamorphic Geology, 25, 703-713, 2007

[13] Harley, S.L., and Nandakumar, V., Accessory Mineral Behaviour in Granulite Migmatites: a Case Study from the Kerala Khondalite Belt, India. Journal of Petrology, 55, 1965-2002, 2014

[14] Weinberg, R.F., and Hasalová, P., Water-fluxed melting of the continental crust: A review. Lithos, 212-215, 158-188, 2015

Pressure-Temperature path of a garnet-biotite-sillimanite gneiss from the Oyayubi ridge, Brattnipene, Sør Rondane Mountains.

Tatsuro ADACHI[1], Tetsuo KAWAKAMI[2], Masaoki UNO[3] and Fumiko HIGASHINO[2]
[1]*Kyushu University,* [2]*Kyoto University and* [3]*Tohoku University*

The Sør Rondane Mountains (SRM) comprise medium to high-grade metamorphic rocks with granitic, syenitic and minor mafic dikes (e.g. Shiraishi et al., 1997). Based on recent metamorphic and geochronological studies, this region is divided into the NE terrane and the SW terrane by the Main Tectonic Boundary (MTB, Osanai et al., 2013). The NE terrane is characterized by clockwise *P-T* path and detrital zircons older than 1200 Ma whereas the SW terrane by counter-clockwise *P-T* path and detrital zircons younger than 1200 Ma (Osanai et al., 2013). Osanai et al. (2013) considered that both terranes have collided at ca. 600-650 Ma during which the thrust up movement of the NE terrane took place over the SW terrane. This tectonic model assumed that the SRM was formed by a single collisional event during ca. 600-650 Ma. Recently, low angle ductile shear zone where pelitic gneisses and felsic gneisses are in contact with each other was found at the eastern slope of the Oyayubi ridge, Brattnipene located in the SW terrane (Adachi et al., 2020). Structurally the pelitic gneisses overlie the felsic gneisses, and the timing of the peak metamorphism of the former is at ca. 600 Ma, but that of the latter is at ca. 550 Ma (Adachi et al., 2021). This indicates that the SRM was formed by at least two different metamorphic events, and it requires building a new tectonic model based on more precise *P-T-t* path. The purpose of this study is to constrain the *P-T* path from the pelitic gneiss of the Oyayubi ridge.

We analyzed a garnet-biotite-sillimanite gneiss (sample no. TA19120703B), which is a thin sillimanite-rich layer intercalated in the pelitic gneisses. This rock is composed of garnet, biotite (X_{Mg}=0.53, TiO_2=1.6 wt %), sillimanite (Fe_2O_3=0.4 wt %), quartz, plagioclase (An_{35}) and minor amounts of ilmenite, rutile, zircon, monazite and apatite in the matrix. Garnet shows chemical zoning with relatively high Ca and Y and low P in the core and the opposite in the rim. The core of garnet ($Alm_{65}Pyp_{28}Grs_6Sps_1$) shows a sector zoning, and contains quartz, rutile and monazite. The rim of garnet ($Alm_{66}Pyp_{29}Grs_4Sps_1$) contains fine-grained sillimanite (Fe_2O_3=1.4 wt %) and ilmenite. Cordierite (X_{Mg}=0.74) and biotite (X_{Mg}=0.55, TiO_2=2.0 wt %) replace the garnet along the crack which is discordant to the foliation of the gneiss. Sillimanite (Fe_2O_3=0.8 wt %) and ilmenite are enclosed in these cordierite and biotite. These cordierite and biotite are partly replaced by chlorite and muscovite. Kyanite and andalusite are only found with these chlorite and muscovite.

The garnet-biotite geothermometer (Holdaway, 2000) and garnet-biotite-plagioclase-quartz geobarometer (Wu et al., 2004) were applied to the rim of garnet and biotite and plagioclase in the matrix, which gave ca. 750 °C and 7 kbar. The temperature condition is consistent with the result of Ti in quartz geothermometer (Wark & Watson, 2006). These conditions can be interpreted as near peak metamorphic conditions. The textures in the gneiss suggest that following reactions occurred after garnet formation:

(1) Grt + Kfs + melt/fluid = Crd + Bt + Qz
(2) Crd + Bt + fluid = Chl + Ms + Qz
(3) Sil = Ky/And

Based on petrogenetic grid for the NaKFMASH and KMASH systems (Spear et al., 1999), reaction (1) occurred during near isothermal decompression process after the peak metamorphic condition. Intimate textural relationship of kyanite, andalusite, chlorite and muscovite suggests that the reactions (2) and (3) occurred approximately at the same timing and *P-T* condition, likely at around the kyanite/andalusite transition condition.

The result of this study shows a decompression *P-T* path after the peak metamorphism in the Brattnipene area, which is inconsistent with the previous studies suggesting that the rocks in the Brattnipene area recorded counter-clockwise *P-T* path. Therefore, precise dating correlating the dates with the rock texture will be conducted near future in order to understand the *P-T-t* history of the SRM.

References

Adachi, T., Kawakami, T., Uno., M., Higashino, F. and Tsuchiya, N., 2020, Contrasting P-T records of the metamorphic rocks at the Oyayubi ridge of Brattnipene, Sør Rondane Mountains, East Antarctica. Abstract for the 11th Symposium on Polar Science, OGo4.

Adachi, T., Kawakami T., Higashino, F. and Uno M., 2021, Geochronology of the metamorphic rocks at the Oyayubi ridge of Brattnipene. Abstract for JpGU 2021 meeting, SMP24-P01

Holdaway, M. J., 2000, Application of new experimental and garnet Margules data to the garnet–biotite geothermometer. American Mineralogist, 85, 881–892.

Osanai, Y., Nogi, Y., Baba, S., Nakano, N., Adachi, T., Hokada, T., Toyoshima, T., Owada, M., Satish-Kumar, M., Kamei, A., Kitano, I., 2013, Geologic evolution of the Sør Rondane Mountains, East Antarctica: Collision tectonics proposed based on metamorphic processes and magnetic anomalies. Precambrian Research, 234, 8-29.

Shiraishi, K., Osanai, Y., Ishizuka, H., Asami, M., 1997, *Antarctic Geological Map Series (Sheet 35, Sør Rondane Mountains)*. National Institute of Polar Research, Japan.

Spear, F., Kohn, M. and Cheney J., 1999, P -T paths from anatectic pelites. Contribution to Mineralogy and Petrology, 134, 17-32.

Wark, D.A. and Watson, E.B., 2006, TitaniQ: a titanium-in-quartz geothermometer. Contribution to Mineralogy and Petrology, 152, 743-754.

Wu, C., Zhang, J. and Ren, L., 2004, Empirical Garnet–Biotite–Plagioclase–Quartz (GBPQ) Geobarometry in Medium- to High-Grade Metapelites. Journal of Petrology, 45, 1907-1921.

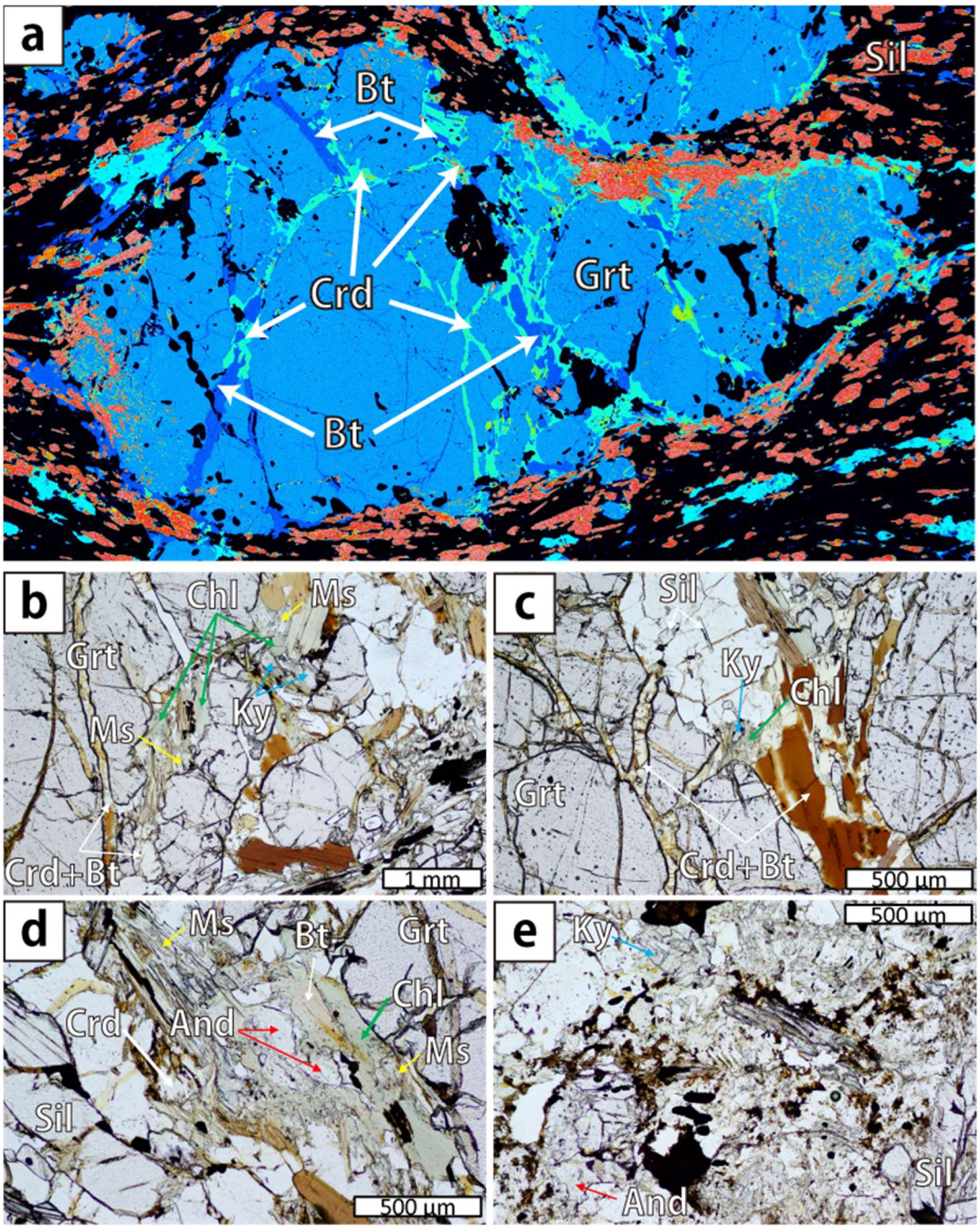

Fig1. Mode of occurrences of key mineral assemblages in the analyzed garnet-biotite-sillimanite gneiss. (a) Crd + Bt replacing Grt along the crack. Crd + Bt are found in the crack which is discordant to the foliation of the gneiss. (b), (c) Chl + Ms replacing Crd + Ms. Ky is also found only with Chl + Ms. (d) And in Chl +Ms. (e) Ky and And found near each other. Ky and And are found only with Chl +Ms, indicating that the formation of Ky, And, Chl and Ms was approximately at the same timing and *P-T* condition.

Highlights of the Student Himalayan Exercise Tour 9 years and invitation to the 10th tour[1].

Masaru Yoshida[2] and Student Himalayan Field Exercise Project[3]

[2] *Gondwana Institute for Geology and Environment, Hashimoto (GIGE), Japan, and Tribhuvan University, Kathmandu, Nepal*

[3] *c/o Gondwana Institute for Geology and Environment, Hashimoto, Japan*

The Himalaya is the best place for the geological field exercise of students; they are sure to be impressed the great beauty of the Himalayan geology as well as the mountainous scenery, and also, feel the movement of the crust, and understands the principal importance of studying geology and geomorphology in the field.

The Student Himalayan Exercise Project[4] has been conducting a two weeks (depart from and return to Japan) Student Himalayan Exercise Tour (SHET) in the Himalayan Orogen with its full traverse from the north to the south in every March since 2012, nominally sponsored by 6 academic societies of Japan and Nepal including IAGR. The exercise tour covers the Tethys Himalayan, Higher Himalayan, Lesser Himalayan, Sub Himalayan and the Gangetic Alluvial zones, observing important geologies of all the geologic zones and boundary major faults, utilizing a specially prepared English exercise guidebook (Yoshida and Ulak, 2017). The tour starts from northernmost Muktinath (3800m asl), the world's very holly temple of Hinduism, passing through Pokhara city, the central of the Himalayan sightseeing and Tansen city, a traditional capital town of old Palpa kingdom, and ends at Lumbini (150m asl), the world's most holly place of Buddhism as the birth place of Buddha. The tour traverses from the tundra zone to subtropical zone within its 250km length of the tour rout. The changing climatic zones reflects dramatic changes of vegetations as well as living styles of human beings. Thus, the tour includes a variety of interests apart from geology as well.

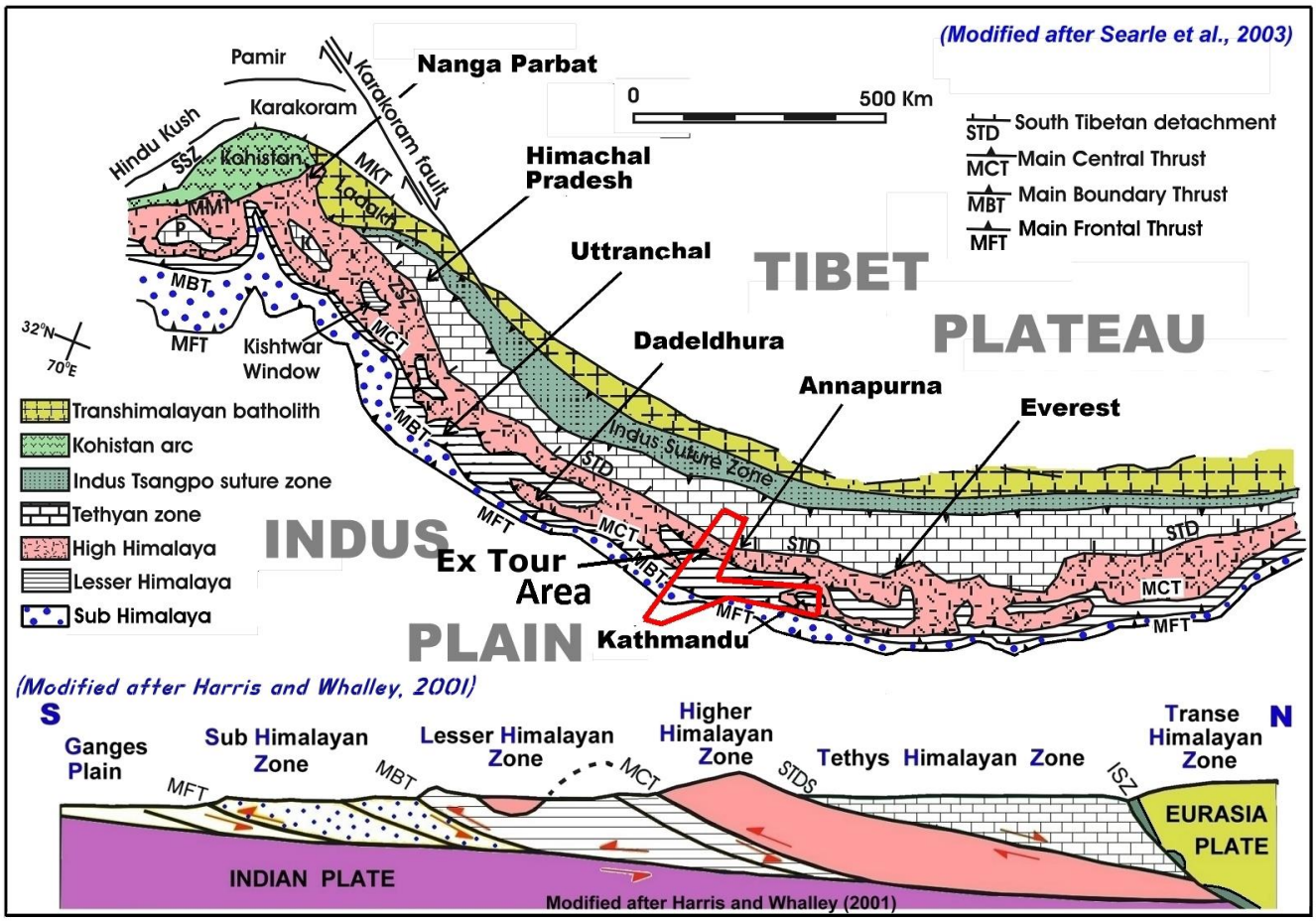

Himalayan geologic outline and the exercise tour area

---

[1] Part of this presentation were delivered in Yoshida et al., 2019, Yoshida., 2020, and Yoshida and Student Himalayan Field Exercise Project, 2021a and b.

[3] Convenors of the Project include M. Yoshida, K. Arita, T. Sakai, and B.N. Upreti.

[4] SHET-HP: http://www.gondwanainst.org/Studentfieldex_index.htm

Before the start and after the end of the tour, a pre-tour seminar and a summary seminar have been organized, held at the Department of Geology, Tri-Chandra Campus, Tribhuvan University (DGTU), Kathmandu, and after the seminars, the participants of the SHET are escorted to city tours by students of the DGTU. Participants of the SHET submit a report of the tour and the tour leader assembles all the reports and tour data and forms a book titled Traversing the Himalayan Orogen 2012 (2013 and so on), and the project has published the book every year (e.g., Yoshida, 2020). All 144 participants of the tour of 9 years evaluated not only the great geology and beauty of the Himalaya but also friendship interaction among participants as well as with students of the DGTU.

The SHET-8 team with the Mustang Himal on the back sight (on the east terrace of Kagbeni, March 2019)

The voluntary leaders and teachers of the exercise tours have included retired and/or active university teachers and office engineers who are experienced in the Himalayan geology as well as field geology. The Gondwana Institute for Geology and Environment (Hashimoto, Japan) has mainly been conducting the organization of the exercise tour, in collaboration with the DGTU.

At the poster presentation, highlight field photos of the exercise tours of past 9 years from 2012 to 2019 will be displayed. A recruit for the 10th SHET to be held in next March will also be delivered.

References

Yoshida, M., Arita, K., Sakai, T., and Upreti, B.N., 2019, Japan-Nepal joint Student Himalayan Exercise Program 7 years. Universal Journal of Geoscience, 7 (1), 15-30.

Yoshida, M., 2020 (Ed.), *Traversing the Himalayan Orogen 2020 - A Record of the 9th Student Himalayan Field Exercise Tour in March 2020 (In Japanese and English).* Field Science Publishers, Hashimoto, Japan, 193 pages.

Yoshida, M. and Student Himalayan Field Exercise Project, 2021a, The Student Himalayan Field Exercise Program VI: Summary of 9 years (in Japanese). Chigaku Kyoiku to Kagaku Undo (Geological Education and Movement), Submitted, August 2021.

Yoshida, M. and Student Himalayan Field Exercise Project, 2021b, Student Himalayan Exercise Program 9 years. Presented at the 18th International Symposium on Gondwana to Asia, held in Qingdao, China, September 2021.

Paleostress inversion in hydro-fractured metamorphic complex using 3D aerophotography images (Sør Rondane Mountains, East Antarctica)

Masaoki UNO[1], Tetsuo KAWAKAMI[2], Tatsuro ADACHI[3], and Fumiko HIGASHINO[2]
[1]*Tohoku University*, [2]*Kyoto University* and [3]*Kyushu University*

Fluid pressure is one of the most important parameters that govern fluid flow in the deep crust. Recent geophysical observations suggest that crustal seismic swarms are associated with migration of pressurized fluid, whose fluid pressure may reach near lithostatic (e.g., Yoshida and Hasegawa, 2018). However, geological observations of such high fluid pressure and its duration in the crust are rather qualitative, and their relations to geophysical observations remain largely unconstrained. Exceptionally well-exposed crustal sections of Sør Rondane Mountains (SRM), East Antarctica provides an excellent opportunity to evaluate the fluid flow in the deep crust. Recent studies have revealed extremely short fluid activities of hours are recorded in the amphibolite-faces reaction zones along mineral-filled fractures in SRM (Mindaleva et al., 2020). Here we show preliminary results of paleostress and fluid pressure inversion of hydro-fractured metamorphic complex, utilizing 3D aerophotography images. Combined with constraints on the duration of fluid activities, we discuss the dynamic behavior of fluids during crustal fracturing.

The Sør Rondane Mountains (SRM) are part of the Pan-African collision zone related to Gondwana amalgamation at ca. 650–500 Ma (Osanai et al., 2013), and are dominated by amphibolite- and granulite-facies metamorphic rocks and granitoids. Previous studies have revealed amphibolite-facies hydration reactions along fractures (Adachi et al., 2010; Higashino et al., 2019; Mindaleva et al., 2020) and Cl-bearing fluid activities during prograde and retrograde metamorphism, that are likely to correlate with km-scale shear zones (Higashino et al., 2013; Kawakami et al., 2017) and igneous activities (Uno et al., 2017).

The study area is located at northeastern part of Mefjell area. Orthopyroxene-bearing felsic gneiss (OFG) are cut by fractures filled with granitic vein, or those filled with biotite and amphibole (m to ~100 m in length; Fig. 1a). Brownish OFG are hydrated along the fractures and form cm– to decimeter–scale whitish reaction zones composed of hornblende-biotite-bearing felsic gneiss

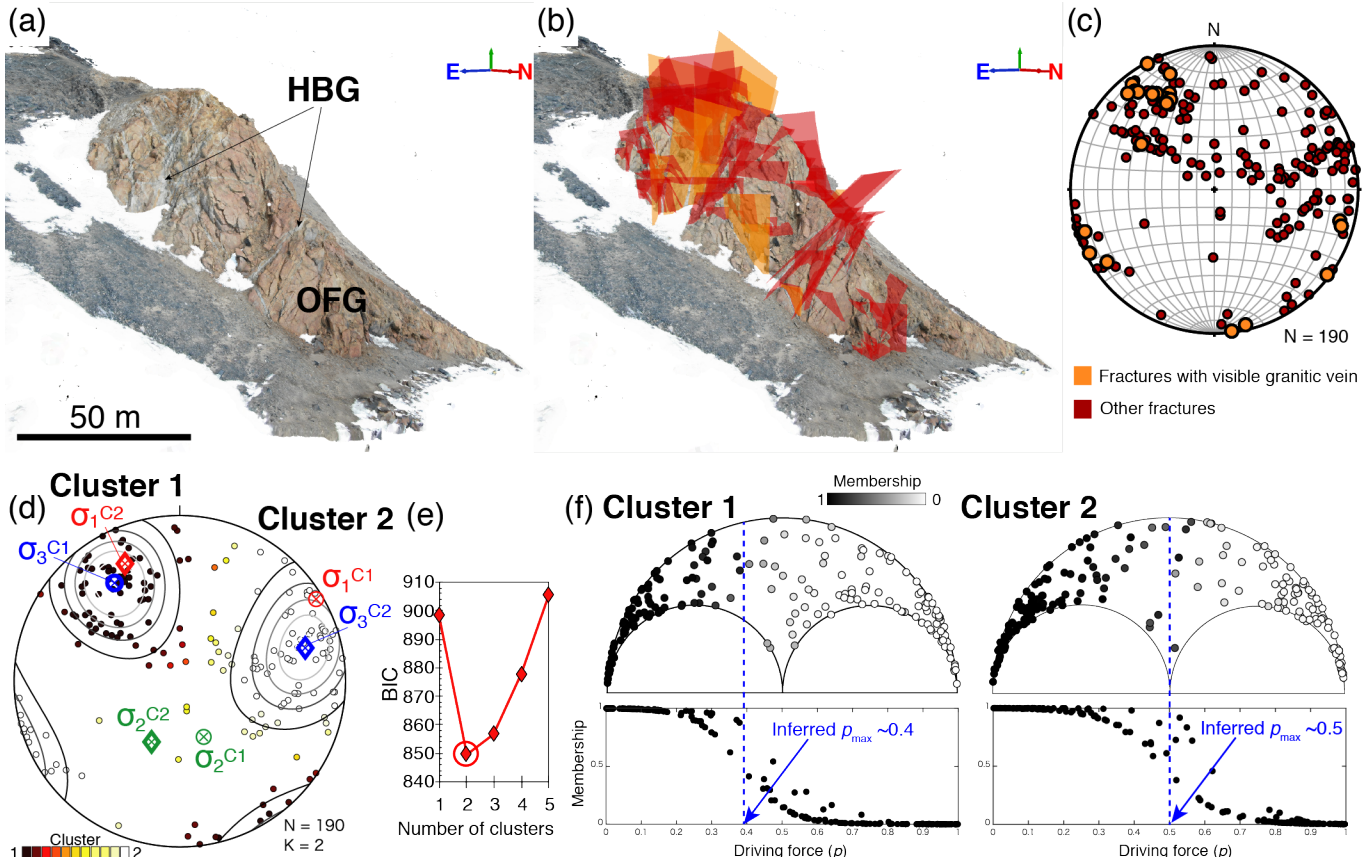

Fig. 1 Occurrence of fractures in the survey area and preliminary results of paleostress analyses. (a) 3D digital model of the outcrop. (b) Fractures identified on the 3D digital model. (c) Lower-hemisphere, equal-area projection for the orientations of the fractures. (d) Clustering results and orientations of the inferred principal stress. Membership (i.e., the probability of a fracture to belong to a certain cluster) is shown by colors. (e) Bayesian information criterion (BIC) as a function of the number of clusters. (f) Mohr diagram and driving pressures of the fractures belonging to the clusters. The normal stress at which the membership declines indicates the maximum driving pressure, *p*.

(HBG). HBG are characterized by complete hydration of orthopyroxene and clinopyroxene to grunerite, hornblende and biotite, representing fluid infiltration at 0.40–0.55 GPa, 600–670°C (Uno et al., 2020). The gneissosity of OFG is oriented to 140–160°/62–74° (dip direction/dip) throughout the outcrop, and is cut by the fractures. All the fractures are straight and planar, indicating that the fractures are not substantially deformed or folded.

The whole outcrop of OFG (120 m × 70 m × 80 m) was photographed by an unmanned aerial vehicle (UAV; i.e., drone). 32 aerophotography images were processed with a commercial photogrammetric software program (Agisoft Metashape Pro) to generate a 3D digital model of the outcrop (Fig. 1a). The strike and dip of the 190 fractures were measured by a conventional 3D processing software. The analyzed fractures include granitic veins, biotite–amphibole veins, and associated whitish HBG reaction zones, but exclude un-mineralized joints (Fig. 1b). The datasets of fracture orientations were further analyzed for paleostress inversion using GArcmB software (Yamaji, 2016; Yamaji and Sato, 2011). The GArcmB software clusters fracture orientations and classifies groups of fractures that formed under certain paleostress conditions. Based on the distribution of fracture orientations in each group, it estimates stress axes and stress ratios of each fracture group. In addition, based on the distribution of estimated stress on Mohr diagrams, it can infer the fluid pressures that dilated these fractures.

The fractures largely orient NE–SW and NW–SE in strike, and dip steeply towards SE and SW, respectively (Fig. 1c). The results of fracture clustering indicate 2 or 3 clusters are appropriate, based on the Bayesian information criterion (BIC; Fig. 1e). The results assuming 2 clusters suggest that fractures are largely classified into a group with NE–SW strike (cluster 1) and one with NW–SE strike (cluster 2) (Fig. 1d). Cluster 1 is characterized by NE subhorizontal σ_1 (dip direction/dip: 59°/5°), SE subvertical σ_2 (157°/60°) and NW oblique σ_3 (326°/30°). Cluster 2 is characterized by NW oblique σ_1 (335°/23°), SE subvertical σ_2 (205°/57°) and ENE oblique σ_3 (75°/23°). The stress ratios $(\sigma_2 - \sigma_3)/(\sigma_1 - \sigma_3)$ for both clusters are ~0.50. The normalized fluid pressure $p = (p_f - \sigma_3)/(\sigma_1 - \sigma_3)$ were inferred as $p \leq$~0.4 and $\leq$~0.5 for the two clusters (Fig 1f).

The above results indicate that the observed fractures are formed mainly under two different stress states. While the orientations of the σ_2 are almost identical among the two stress states, those of σ_1 and σ_3 switches between the two states (Fig. 1d). Fractures filled with granitic veins and those filled biotite and amphibole were observed for both clusters (Fig. 1b), indicating that both clusters were associated with magmatic and hydrothermal activities. Outcrop observation indicates that the fractures belonging to the two clusters crosscut each other. Previous reactive-transport analyses of HBG had shown that fluid activity during the formation of individual biotite-amphibole-filled fracture is geologically short, and is on the order of ~hours (Uno et al., 2021 JpGU abstract). These results suggest that local stress states had repeatedly switched during the hydrofracturing associated with magmatic intrusion in the middle crust.

References

Adachi, T., Hokada, T., Osanai, Y., Toyoshima, T., Baba, S., Nakano, N., 2010. Titanium behavior in quartz during retrograde hydration: Occurrence of rutile exsolution and implications for metamorphic processes in the Sør Rondane Mountains, East Antarctica. Polar Sci. 3, 222–234.

Higashino, F., Kawakami, T., Satish-Kumar, M., Ishikawa, M., Maki, K., Tsuchiya, N., Grantham, G.H., Hirata, T., 2013. Chlorine-rich fluid or melt activity during granulite facies metamorphism in the Late Proterozoic to Cambrian continental collision zone-An example from the Sør Rondane Mountains, East Antarctica. Precambrian Res. 234, 229–246.

Higashino, F., Kawakami, T., Tsuchiya, N., Satish-Kumar, M., Ishikawa, M., Grantham, G., Sakata, S., Hirata, T., 2019. Brine Infiltration in the Middle to Lower Crust in a Collision Zone: Mass Transfer and Microtexture Development Through Wet Grain-Boundary Diffusion. J. Petrol. 60, 329–358.

Kawakami, T., Higashino, F., Skrzypek, E., Satish-Kumar, M., Grantham, G., Tsuchiya, N., Ishikawa, M., Sakata, S., Hirata, T., 2017. Prograde infiltration of Cl-rich fluid into the granulitic continental crust from a collision zone in East Antarctica (Perlebandet, Sør Rondane Mountains). Lithos 274–275, 73–92.

Mindaleva, D., Uno, M., Higashino, F., Nagaya, T., Okamoto, A., Tsuchiya, N., 2020. Rapid fluid infiltration and permeability enhancement during middle–lower crustal fracturing: Evidence from amphibolite–granulite-facies fluid–rock reaction zones, Sør Rondane Mountains, East Antarctica. Lithos 372–373, 105521.

Osanai, Y., Nogi, Y., Baba, S., Nakano, N., Adachi, T., Hokada, T., Toyoshima, T., Owada, M., Satish-Kumar, M., Kamei, A., Kitano, I., 2013. Geologic evolution of the Sør Rondane Mountains, East Antarctica: Collision tectonics proposed based on metamorphic processes and magnetic anomalies. Precambrian Res. 234, 8–29.

Uno, M., Okamoto, A., Tsuchiya, N., 2017. Excess water generation during reaction-inducing intrusion of granitic melts into ultramafic rocks at crustal P–T conditions in the Sør Rondane Mountains of East Antarctica. Lithos 284–285, 625–641.

Yamaji, A., 2016. Genetic algrithm for fitting a mixed Bingham distribution to 3D orientations: a tool for the statistical and paleostress analyses of fracture orientations. Isl. Arc 25, 72–83.

Yamaji, A., Sato, K., 2011. Clustering of fracture orientations using a mixed Bingham distribution and its application to paleostress analysis from dike or vein orientations. J. Struct. Geol. 33, 1148–1157.

Yoshida, K., Hasegawa, A., 2018. Hypocenter Migration and Seismicity Pattern Change in the Yamagata-Fukushima Border, NE Japan, Caused by Fluid Movement and Pore Pressure Variation. J. Geophys. Res. Solid Earth 123, 5000–5017.

Estimation of Shirase Glacier flow velocity from 2018 to 2021 using Sentinel-1 data

Shotaro Ohkawa[1], Koichiro Doi[1,2], Kazuki Nakamura[3], and Hiroto Nagai[4]

[1] *Department of Polar Science, The Graduate University for Advanced Studies*
[2]*National Institute of Polar Research*
[3]*College of Engineering, Nihon University*
[4]*School of Education, Waseda University*

The ice mass discharge is one of the essential parameters in estimating the mass balance of the Antarctic ice sheet, and it is essential to observe the flow velocity of glaciers to estimate the discharge. Therefore, understanding the glacier flow velocity can contribute to the understanding of ice sheet discharge in Antarctica. This study focuses on Shirase Glacier located in East Antarctica. Shirase Glacier is known as one of the fastest flowing Antarctic glaciers. In this presentation, we present the Shirase Glacier flow velocities estimated by applying offset tracking technique to Sentinel-1 Synthetic Aperture Radar (SAR) data.

The flow velocities estimation was applied an offset tracking to SAR data of 94 scenes acquired by the Sentinel-1A from July 2018 to September 2021. We used the Ground Range Detected (GRD) of the Sentinel-1A product which has a pixel spacing of 10 m both range and azimuth directions with a repeat cycle is 12 days. The offset tracking analysis used the GAMMA SAR Processor of GAMMA REMOTE SENSING (Switzerland).

We set up three streamlines which were east, center and west of the Shirase Glacier based on the shape and calculated the flow velocity along each streamline (Figure 1). The green line in Figure 1 shows the location of the grounding line (GL) by Rignot et al. (2011). The estimated flow velocity from the 12 days difference was converted to an annual flow velocity. Depending on the image pair used for offset tracking analysis, it is not always possible to determine the glacier flow velocity accurately. In order to remove the inaccurate values, we performed the following processing. First, the median and standard deviation (SD) were determined from all estimated flow velocity values every 12 days from 2018 to 2021 for each pixel. Then, only values within the median ± SD were used to determine the flow velocity (cf. Mouginot et al., 2017).

Formal error of the estimated displacement by offset tracking analysis is considered to be equivalent to the accuracy of matching the two images (e.g., Nakamura et al., 2016). The accuracy of the two-image matching is within the standard deviation of 0.1-pixel, which corresponds to 1.4 m for Sentinel-1A. In terms of velocity, it is 1.4 m 12-day^{-1}, which is equivalent to 0.04 km year^{-1}. Therefore, the estimation error of the flow velocity by the offset tracking analysis is considered to be approximately 0.04 km year^{-1}.

Figure 2 shows the result of the annual flow velocity at the GL of the Shirase Glacier, which was estimated to be 2.21 ± 0.04, 2.22 ± 0.04, 2.19 ± 0.04 and 2.17 ± 0.04 km year^{-1} in 2018, 2019, 2020 and 2021, respectively. The comparison between the previous and present studies shows the annual flow velocity of the Shirase Glacier at the GL was almost not changed, but that velocity was about 0.1 km year^{-1} slower than that in 2014-2015. The floating ice tongue of the Shirase Glacier has elongated over the past five years. We believe that the elongation of the ice floating ice tongue produces a buttressing effect, which reduces the flow velocity at the GL.

The profile of flow velocity along the streamline from the grounding line to the glacier terminus is shown in Figure 3. The flow velocity in 2018 showed that the flow in the shaded area shown in Figure 3 was about 0.1-0.2 km/year faster than that in 2019 and 2020. In particular, a comparison of the velocity profiles for the period July-December of each year (bottom right of Figure 3) shows a gradual decrease in flow velocity from 2018 to 2020. This result appears to be related to sea ice extent in front of the glacier, but it is a subject for future research.

Acknowledgment
This study was partially supported by JSPS KAKENHI Grant No. 17H06321 and 21K12214.

References

Nakamura, K., Doi, K., Shibuya, K., 2007. Estimation of seasonal changes in the flow of Shirase Glacier using JERS-1 / SAR image correlation. Polar Sci. 1, 73-83.

Nakamura, K., Doi, K., Shibuya, K., 2010. Fluctuations in the flow velocity of the Antarctic Shirase Glacier over an 11-year period. Polar Sci. 4, 443–455.

Nakamura, K., Yamanokuchi, T., Doi, K., Shibuya, K., 2016. Net mass balance calculations for the Shirase Drainage Basin, east Antarctica, using the mass budget method. Polar Sci. 10, 111–122.

Nakamura, K., Yamanokuchi, T., Aoki, S., Doi, K., Shibuya, K., 2017. Temporal variation in the flow velocity for Shirase Glacier in Antarctica over a 20-year period. Seppyo. 79, 3-15.

Pattyn, F., Derauw, D., 2002. Ice-dynamic conditions of Shirase Glacier, Antarctica, inferred from ERS SAR interferometry. J. Glaciol. 48, 559–565.

Rignot, E., J. Mouginot, and B. Scheuchl. 2011. Antarctic Grounding Line Mapping from Differential Satellite Radar Interferometry, Geophysical Research Letters, 38, L10504

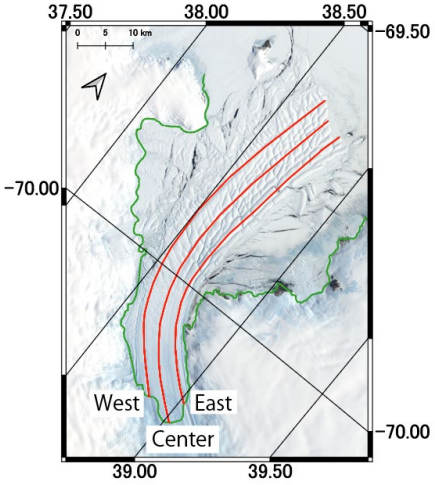

Figure 1. Measurment places of Shirase Glacier. Green line is the GL (Rignot et al., 2011). Red line is the streamlines.

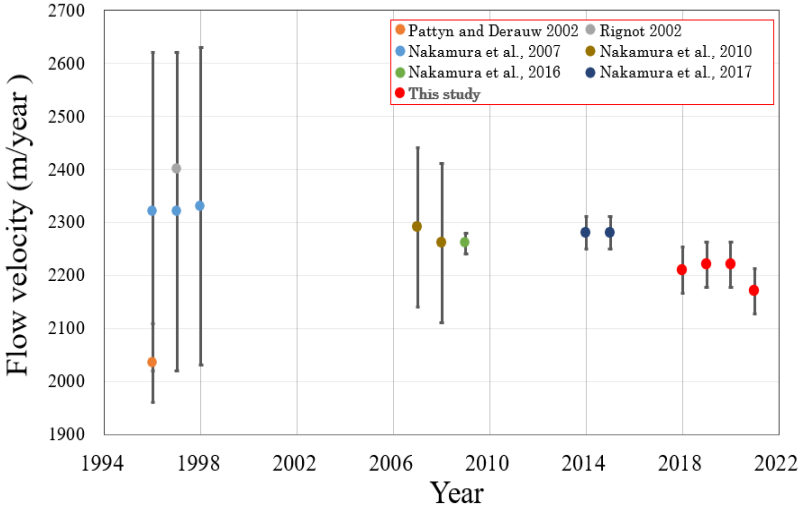

Figure 2. Comparison of the flow velocity of Shirase Glacier at the GL with previous studies.

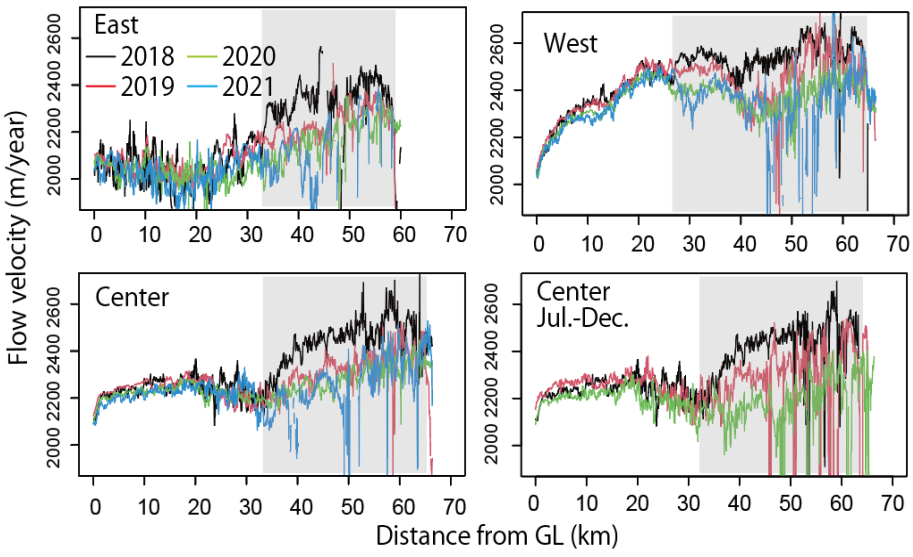

Figure 3. The flow velocities of the Shirase Glacier along the streamlines indicated by red lines in Figure 1.

Episodes of West Antarctic Ice Sheet retreat during Pliocene warmth revealed by a sedimentary record from the Amundsen Sea

Keiji Horikawa[1], Masahiro Noda[2], Miyu Fujimoto[2], Yoshihiro Asahara[3], Ki-Cheol Shin[4], Masao Iwai[5], Li Wu[6], Ellen Cowan[7], Christine Siddoway[8], Claus-Dieter Hillenbrand[9], IODP Expedition 379 Scientists

[1]*Faculty of Science, Academic Assembly, University of Toyama*
[2]*Graduate School of Science and Engineering (Science), University of Toyama*
[3]*Department of Earth and Environmental Sciences, Graduate School of Environmental Studies, Nagoya University*
[4]*Research Institute for Humanity and Nature*
[5]*Center for Advanced Marine Core Research, Kochi University*
[6]*State Key Laboratory of Marine Geology, Tongji University*
[7]*Department of Geological and Environmental Sciences, Appalachian State University*
[8]*Department of Geology, Colorado College*
[9]*British Antarctic Survey*

The ice draining into the Amundsen Sea Embayment in West Antarctica is currently being lost at an accelerated pace, compared to other drainage sectors of Antarctica (e.g., Rignot et al., 2019). From presently observed evidences, ice loss in the Amundsen Sea sector is hypothesized to be a precursor for major West Antarctic Ice Sheet (WAIS) retreat or even WAIS collapse, similar to the major WAIS deglaciation that occurred during Pliocene (5.3–2.6 Ma) (DeConto and Pollard, 2016). In addition, if vast amounts of meltwater released during a WAIS collapse were advected by the westward coastal current to the Wilkes Land margin of East Antarctica, the formation of dense shelf water there would have been weakened, and instead relatively warm Circumpolar Deep Water would have been directed far onto the shelf, triggering additional melting in the Wilkes Land drainage sector of the East Antarctic Ice Sheet.

In this study, we consider that melting of the ice in the Amundsen Sea sector of the WAIS caused the release of a huge freshwater reservoir into the Southern Ocean, which subsequently influenced ocean circulation and ice sheet retreat around both the West and the East Antarctic margin. To trace the behavior of the Amundsen Sea drainage basin during Pliocene warmth, we have analyzed detrital lead (Pb) isotopes on deep-sea sediments (IODP Expedition 379 Site U1532; Gohl et al., 2021) and utilized them as a geochemical tracer of sediment provenance (Fig. 1). Pb isotopes were measured on the < 63μm grain size fraction (i.e., clay and silt) of U1532 sediments and also on bulk rocks collected in western Antarctica (provided by the OSU Polar rock repository, https://prr.osu.edu) to map potential source regions for the detritus. Site U1532 was drilled at a water depth of ~4000 m on Resolution Drift offshore from the eastern Amundsen Sea Embayment. The total length of the cores at Site U1532 is ~780 m, and their sedimentary record spans continuously the time period back to ~6 Ma. More than ten biogenic bearing and partly bioturbated ice-rafted debris (IRD) units intercalated with thick sequences of terrigenous laminated silty clay occur in the Pliocene record. These repeated IRD units in the U1532 cores are also characterized by a predominance of open water diatoms (*Fragilariopsis barronii*, *Dactyliozolen antarcticus*, etc), which suggests that the IRD units reflect relatively warm periods when at least the marine-terminating Amundsen Sea drainage sector of the WAIS collapsed. The Pliocene IRD units show distinctly lower Pb isotope values than the fine-grained laminated sediments above and below them, indicating a tight coupling between changes in sediment provenance and ice loss in the Amundsen Sea sector. In our presentation, we will show the down-core Pb isotope data of the Pliocene section of Site U1532 and the Pb isotope provenance map of western Antarctica created for this study. In combination, these data indicate repeated major WAIS retreats during the deposition of the IRD units.

References

DeConto, R. M., & Pollard, D. (2016). Contribution of Antarctica to past and future sea-level rise. *Nature, 531*(7596), 591-597.

Gohl, K., et al. (2021). Evidence for a highly dynamic West Antarctic Ice Sheet during the Pliocene. *Geophysical Research Letters, 48*(14).

Rignot, E., Mouginot, J., Scheuchl, B., van den Broeke, M., van Wessem, M. J., & Morlighem, M. (2019). Four decades of Antarctic Ice Sheet mass balance from 1979-2017. *Proc Natl Acad Sci U S A, 116*(4), 1095-1103.

Sea-level changes in East Antarctica based on glacial isostatic adjustmet modeling since the Last Interglacial period

Takeshige Ishiwa[1], Jun'ichi Okuno[1,2] and Yusuke Suganuma[1,2]

[1]*National Institute of Polar Research, Research Organization of Information and Systems*

[2]*Department of Polar Science, School of Multidisciplinary Sciences, The Graduate University for Advanced Studies*

Further understanding of the Antarctic Ice Sheet's response to global climate changes requires accurate reconstruction of ice-sheet changes in hundreds -ten thousand years time scale. Field-based evidence of ice-sheet and sea-level changes is useful to reconstruct this longer time scale variability. However, the erosive nature of ice-sheet expansion makes it challenging to obtain this field-based evidence before the Last Glacial Maximum. Sedimentary records from Lützow–Holm in East Antarctica show that the sea level during Marine Isotope Stage 3 was close to the present level. Predicted sea level by glacial isostatic adjustment modeling hardly explains these sea-level data. Including this problem, we will present sea-level changes in Lützow–Holm since the Last Interglacial based on a comparison of glacial isostatic adjustment modeling with reported sea-level observations.

References

Ishiwa, T., Okuno, J., Suganuma, Y. Excess ice loads in the Indian Ocean sector of East Antarctica during the last glacial period. Geology (2021) 49 (10): 1182–1186.

Barberton impact spherules, South Africa: pursuing of shock metamorphism by using Raman spectroscopy

Árpád Csámer[1], Diána Skita[1], István Rigó[2], Miklós Veres[2], Péter Futó[1], József Vanyó[3], Arnold Gucsik[1,3]
[1]*Cosmochemistry Research Group, University of Debrecen, Hungary*
[2]*Applied and Nonlinear Optics Research, Wigner Research Centre for Physics, Hungary*
[3]*Research Group of the Planetary Sciences and Geodesy, Eszterházy Károly University, Hungary*

Barberton greenstone belt (South Africa) contains the remnants of the oldest (3.5 - 3.25 Ga) impact event on the Earth. The greenstone belt is composed of volcanic and volcaniclastic rocks, cherts, and siliciclastic sedimentary rocks arranged in three major lithostratigraphic units: from the base to top the Onverwacht Group, Fig Tree Group, and the Moodies Group. In this rock series, four distinct layers consisting of millimeter-sub millimeter size spherical fragments called spherules can be found, namely the S1, S2 S3, and S4, respectively. The spherules contain primary and secondary minerals, such as microcrystalline quartz, phyllosilicates, anatase, rutile, and spinel. Shukolyukov et al. (2000) and Kyte et al. (2003) revealed chromium isotope anomaly in the spherule layers interpreted as an indicator of a carbonaceous chondritic projectile. Based on the uncommon Cr isotope ratio, as well as the elevated Ir concentration (Koeberl and Reimold, 1995) of the spherule layers, the impact-related origin is presumed (e.g., Krull-Davatzes et al. 2006) however, some authors argue proposing a volcanic origin at least for some of the layers (e.g., Koeberl and Reimold, 1995, Hofmann et al. 2006). By all means, Hofmann et al. (2006) drew the attention that many questions are unanswered regarding the formation and origin of the Barberton spherule layers. One of the well-known criteria to identify impact events is to detect the effect of shock metamorphism, and this study aims to examine the structural composition of the spherules by using Raman spectroscopy.

Our proposed systematic work is based on multiple technological approaches, which were published by Gucsik et al. (2004), as follows. Gucsik et al. (2004) utilized scanning electron microscope and micro-Raman spectroscopy studies to identify shock-induced amorphization in the impact-derived glasses, such as Muong-Nong-type tektite, Aouelloul impact glass, and Libyan desert glass. They found a shock indicator in those impact glasses, which is a fused silica-glass (lechatelierite).

As an impactor for the Barberton spherules, a bolide with 20-50km diameter was suggested (Byerly and Lowe 1994, Shukolyukov et al., 2000; Kyte et al., 2003). The impact of such a large body may trigger shock-wave-related heating and deformation with a temperature of 2500-3000 C and a peak pressure of 50-60 GPa, resulting in the formation of lechatelierite (impact-derived glass). The Raman spectrum can indicate the presence of the remnant of the earlier silicate minerals and the lechatelierites in shock-metamorphosed tektites. Also, it can help us to separate the shocked glass from other silicate phases, such as natural amorphous volcanic glass.

Rock samples from the Barberton greenstone belt spherule layers (Figure 1) were analyzed by laser Raman microscope at the Applied and Nonlinear Optics Research, Wigner Research Centre for Physics (Hungary) to investigate the effect of the shock-metamorphism. Our results are compared to the Raman spectra of natural volcanic and proven impact glass samples to observe the similarities and differences in the silicate structures.

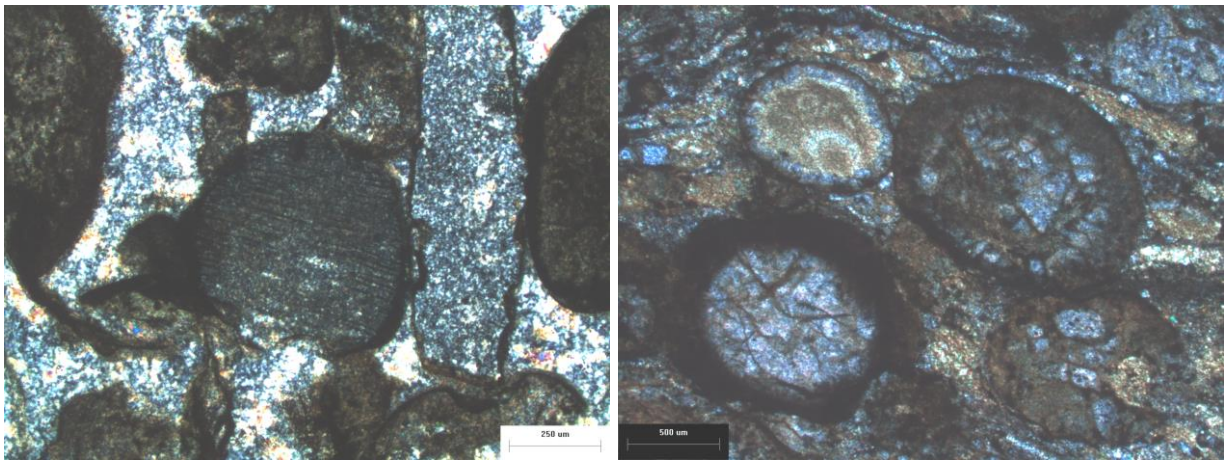

Figure 1. Photomicrographs of spherules in the sample F2 and F26A from the Barberton greenstone belt

References

Byerly, G.R. and D.R. Lowe, Spinel from Archean impact spherules, Geochimica et Cosmochimica Acta, 58, 3469-3486, 1994.

Hofmann, A., W.U. Reimold and C. Koeberl, Archean spherule layers in the Barberton greenstone belt, South Africa: A discussion of problems related to the impact interpretation, Geological Society of America, Special Paper, 405, 33-56, 2006.

Gucsik, A., C. Koeber, F. Brandstätter, E. Libowitzky and M. Zhang, Infrared, Raman, and cathodoluminescence studies of impact glasses, Meteoritics & Planetary Science 39(8), 1273–1285, 2004.

Koeberl, C. and W.U. Reimold, Early Archaean spherule beds in the Barberton Mountain Land, South Africa: No evidence for impact origin, Pre-cambrian Research, 74, 1-33, 1995.

Krull-Davatzes, E.A., D.R. Lowe and G.R. Byerly, Compositional grading in an ~3.24 Ga impact-produced spherule bed, Barberton greenstone belt, South Africa: A key to impact plume evolution, South African Journal of Geology, 109, 233-244, 2006.

Kyte, F.T., A. Shukolyukov, G.W. Lugmair, D.R. Lowe and G.R. Byerly, Early Archean spherule beds: Chromium isotopes confirm origin through multiple impacts of projectiles of carbonaceous chondrite type, Geology, 31, 283-286, 2003.

Shukolyukov, A., F.T. Kyte, G.W. Lugmair, D.R. Lowe and G.R. Byerly, Early Archean spherule beds: Confirmation of impact origin, Meteoritics and Planetary Science, 35, supplement S, A146-A147, 2000.

Absolute Gravity Measurements Planned in JARE63

Koichiro Doi[1,4], Akito Araya[2], Daisuke Oka[3], Yoichi Fukuda[1], Yuichi Aoyama[1,4], Jun'ichi Okuno[1,4], Akihisa Hattori[4]
[1]*National Institute of Polar Research*
[2]*Earthquake Research Institute, The University of Tokyo*
[3]*Hokkaido Research Organization*
[4]*The Graduate University for Advanced Studies, SOKENDAI*

Following to the absolute gravity measurements carried out at JARE59, we plan to conduct absolute gravity measurements at Syowa Station and three field sites, that is, Langhovde, Skarvsnes and Rundvagshetta, as an scientific reasearch activity in JARE63. In the previous measurements at JARE59, we carried out absolute gravity measurements at Syowa Station and six sites (Langhovde, Skallen, Rungvagshetta, Botnnuten, Akarui-Misaki, Mt. Riiser-Larsen) in the field, and determined the gravity values at each sites. Two absolute garvimeters FG-5 and A10 were used for gravity measurement in Syowa Station and A10 for the measurements in the field.

In the measurement at JARE63, we will use four free-fall type absolute gravimeters, FG-5, A10, TAG-1 and TAG-2. In addition, the Geospatial Information Authority of Japan (GSI) also brought in two absolute gravimeters (FG-5 and AQG) for measurement. The absolute gravimeters TAG-1 and TAG-2 were newly developped at the Earthquake Research Institute of the University of Tokyo. They were developped for the measurements at multiple points in the field, and the sizes are smaller than A10.

In the first half of the summer operation of JARE63, we will perform comparative measurements using four gravimeters, and in the second half, we will perform field measurements using other gravimeters than FG-5.There are two gravity measurement basements in Gravity Hut at Syowa Station, and six gravimeters including two gravimeters brought by GSI will take turns to use the two basements for the measurement. Figure 1 shows the test measurement conducted at the Ishioka Geodetic Observatory of GSI before the departure of JARE63.

If the measurement at JARE63 is carried out with good accuracy, the third measurement at Langhovde will be able to determine the gravity change there. In addition, if the results of TAG-1 and TAG-2 are in good agreement with those of other gravimeters, we will have more choices of gravimeters for the future gravity measurements in Antarctica.

Figure 1. Test measurement at the Ishioka Geodetic Observatory of GSI.

Geochronological and petrogenesis of charnockite from Mt. Cronus, Napier Complex, Enderby Land, East Antarctica

Miku Endo[1], Kenichiro Tani[2] and Shin-ichi Kagashima[1]
[1] *Faculty of Science, Yamagata University*
[2] *Department of Geology and Paleontology, National Museum of Nature and Science*

This study refers to the tectonic events that occurred at Mt. Cronus, located in the UHT metamorphic region in the interior of the Napier Complex from the Meso Archean to Paleo Proterozoic.

The following age values obtained in the analysis and three tectonic events reported by previous studies are discussed in separate sections.

(1) ca. 2800 Ma: high grade metamorphism
(Hokada et al., 2003; Kelly and Harley, 2005)

(2) 2630 Ma: Consistency of age with other area in the Napier Complex
(Horie et al., 2012)

(3) ca. 2500 Ma: UHT metamorphism
(Hokada et al., 2003; Kelly and Harley, 2005)

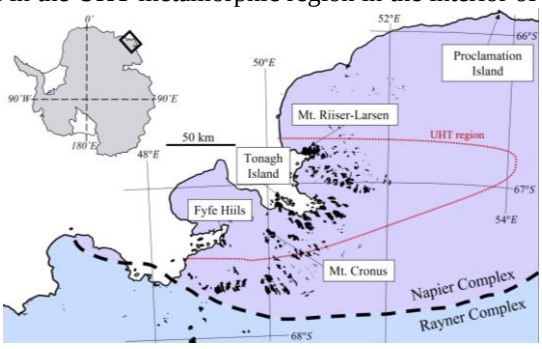

Fig. 1:geological outline of the Napier Complex

The Napier Complex is Archean granulite-facies craton block composed of a variety of granitic metamorphic rocks that make up the granulite facies. An experienced a variety of tectonothermal events such as in the UHT in the latest Archean. It is considered to have undergone at least two advanced metamorphic events at ~2.8 Ga and ~2.5 Ga (Kelly and Harley, 2005). The mineral assemblage is sapphirine + quartz, osumiite, high Al orthopyroxene, or high Ca mesoparsite, which is estimated to have undergone UHT conditions with metamorphic temperatures of 1050-1120°C and peak temperatures of 1100°C or higher, and pressures of 7-11 kbar, increasing from north to south (Dallwitz, 1968; Harley, 1987; Hensen and Motoyoshi, 1992; Harley and Motoyoshi, 2000; Hokada, 2001; Ishizuka et al.2002). Using SHRIMP zircon U-Pb dating a protolith age about 3870-3770 Ma was reported for a tonalitic gneiss from Mt. Sones (Harley and Black, 1997) and about 3850 Ma from the granitic gneiss of Gage Ridge (Kelly and Harley, 2005). However, the majority of the Napier Complex is estimated to have formed during the middle to late Archean (ca. 3300-2600 Ma).

In this study, we use charnockite samples collected from Mt. Cronus during JARE46 (Fig. 1). This have a medium- to fine-grained gneissosity. The major minerals are quartz, plagioclase, orthopyroxene, K-feldspar, biotite, and accessory minerals are garnet, zircon, apatite, and monazite. The analytical method is U-Pb dating of zircon using LA-ICPMS.

In this study, we obtained a wide range of ages from 2828 to 2148 Ma. This suggests that a variety of tectonothermal events occurred. The Th/U ratio of the samples have a wide range from 0.08-0.73, which suggests a strong influence by the secondary formation of surrounding minerals such as monazite and apatite.

However, we could not obtain values for the pre-3.0 Ga protolith forming age recorded by felsic orthogneisses and paragneisses in previous studies. Similarly, no pre-3.0 Ga ages have been reported for the $^{207}Pb/^{206}Pb$ zircons of the Garnet-absent charnockite of Proclamation Island, which is located outside the UHT metamorphic region in the northern part of the Napier Complex (Kelly and Harley. 2005). Charnokitization under high-temperature conditions is assumed to be a separate event from the pre-3.0 Ga protolith formation event. 2988±23 Ma is the oldest age of the Garnet-absent charnockite from Proclamation Island. Inherited zircon of metasedimentary gneiss from Zircon Point has an age of 2855 Ma. As in the case of the igneous zircon of tonalite from Mt. Riiser-Larsen which formed at about 2830 Ma (Hokada et al., 2001), an event of about 2800 M is considered to have occurred in a northeast-southwest direction. The oldest age in this study is 2828±16 Ma, which provides evidence that the sequence of events that began at about 2990 Ma was also occurring at Mt. Cronus, which is located inland.

(1) ca. 2800 Ma: high grade metamorphism

The age range of the protolith rock formation obtained from the analysis is about 2828-2753 Ma. This is the region of ossilatory zoning and vague "fir-tree" zoning obtained from CL images of zircons. This age value is thought to reflect the age of high grade metamorphism, which occurred at ca. 2.8 Ga (Kelly and Harley, 2005, Hokada et al., 2003). Based on the zoning pattern of the CL images, we propose that the protolith rocks were formed as anatexis melts during the high metamorphism of 2.8 Ga in the Napier Complex. A pressure of ~8-11 kbar, which is a relatively low pressure environment, was posed (Kelly and Harley, 2005). This pressure is reasonable considering the environment of metamorphism of charnockite and granulite phases.

(2) 2630 Ma: Consistency of age with other sites in the Napier Complex

A concentration of ages is also observed at about 2630 Ma. The age concentration at 2630 Ma is consistent with those of other sites in the Napier Complex, such as Mt. Riiser-Larsen (Suzuki et al., 2006), Tonagh Island (Carson et al., 2002a), and Fyfe Hiils (Horie et al., 2012). Therefore, the coincidence of age values in the inland area suggests that this was a large-scale tectonic event in the Napier Complex.

(3) ca. 2500 Ma: UHT metamorphism

The greatest concentration of ages is found at ca. 2490-2440 Ma. This region accounts for about 24.4 % of the analyzed points. The CL image shows that it is more pronounced on the bright and broad rim, and also on the broad rim with overgrowth (Fig. 2). This is the last event that is thought to have been caused by the UHT metamorphism at the end of the latest Archean (ca. 2500 Ma). The broad, bright rim of several tens of micrometers in width suggests a long metamorphic period.

The subsequent relatively young ages of 2267 Ma and 2148 Ma may reflect local events such as alteration and deformation associated with later pegmatite formation.

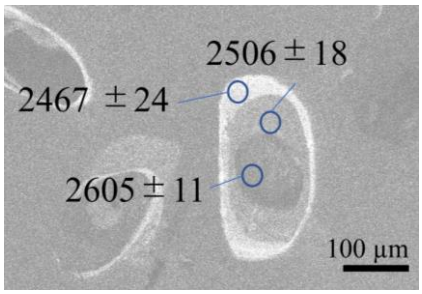

Fig. 2: Zircon CL image

References

Carson, C.J., Ague, J.J., Coath, C.D., U–Pb geochronology from Tonagh Island, East Antarctica: implications for the timing of ultra-high temperature metamorphism in the Napier Complex. Precambrian Research, 116, 237–263, 2002a.

Dallwitz, W. D., Coexisting sapphirine and quartz in granulite from Enderby Land, Antarctica. Nature, 219, 476-477, 1968.

Harley, S. L., A pyroxene-bearing meta-ironstone and other pyroxene granulite from Tonagh Island, Enderby Land, Antarctica: further evidence for very high temperature (>980°C) Archaean regional metamorphism in the Napier Complex. Journal of Metamorphic Geology, 5, 341-356, 1987.

Harley, S. L. and Black L. P., A revised Archaean chronology for the Napier Complex, Enderby Land, from SHRIMP ion-microprobe studies. Antarctic Science, 9, 74-91, 1997.

Harley, S. L. and Motoyoshi, Y., Al zoning in orthopyroxene in a sapphirine quartzite: evidence for >1120°C UHT metamorphism in the Napier Complex, Antarctica, and implications for the entropy of sapphirine. Contributions to Mineralogy and Petrology. 138, 293-307, 2000.

Hensen, B. J. and Motoyoshi, Y., Osumilite-producing reactions in high-temperature granulites from the Napier Complex, East Antarctica: tectonic implications. In: Yoshida Y, Kaminuma K, Shiraishi K. (eds) Recent progress in Antarctic Earth Science. Terra Scientific Publishing Company, Tokyo, 87-92, 1992.

Hokada, T., Feldsper thermometry in ultrahigh-temperature metamorphic rocks: Evidence of crustal metamorphism attaining ~1100°C in the Archean Napier Complex, East Antarctica. American Mineralogist, v. 86, 932-938, 2001.

Hokada, T., Misawa, K., Shiraishi, K., and Suzuki, S., Mid to late Archaean (3.3-2.5 Ga) tonalitic crustal formation and high-grade metamorphism at Mt. Riiser-Larsen, Napier Complex, East Antarctica. Precambrian Research, 127, 215-228, 2003.

Hokada, T., Motoyoshi, Y., Suzuki, S., Ishikawa, M. and Ishizuka, H. Geodynamic evolution of Mt. Riiser-Larsen, Napier Complex, East Antarctica, with reference to the UHT mineral associations and their reaction relations. In: Satish-Kumar, M., Motoyoshi, Y., Osanai, Y., Hiroi, Y., Shiraishi, K. (Eds.), Geodynamic evolution of East Antarctica: a key to the East–West Gondwana Connection: Geological Society, London, Special Publications, 308, 253–282, 2008.

Horie, K., Hokada, T., Hiroi, Y., Motoyoshi, Y. and Shiraishi, K. Contrasting Archaen crustal records in western part of the Napier Complex, East Antarctica: New constraints from SHRIMP geochronology. Gondwana Res., v.21, 829-837, 2012.

Ishizuka , H., Suzuki, S., Nakamura, A., Peak temperatures of ultra-high temperature metamorphism of the Napier Complex, Enderby Land, East Antarctica, as deduced from porphyroclastic pyroxenes of meta-ultramafic rocks. Polar Geoscience, 15, 1-16, 2002.

Kelly, N.M. and Harley, S. L., An integrated microtextural and chemical approach to zircon growth at >1000 °C. Contributions to Mineralogy and Petrology, 149, 57-84, 2005.

Suzuki, S., Arima, M., Williams, I.S., Shiraishi, K., and Kagami, H., Thermal history of the UHT metamorphism in the Napier Complex, East Antarctica: insights from zircon, monazite, and garnet ages. Journal of Geology, 114, 65–84, 2006

Unveiling seafloor spreading mode and geodynamics in the Southeast Indian Ridge: New challenge in Japanese Antarctic Research Expedition

Masakazu Fujii[1,2]

[1] *National Institute of Polar Research, Tachikawa, Japan*

[2] *SOKENDAI (The Graduate University for Advanced Studies), Hayama, Japan*

Understanding the evolution of ocean basins is critical for revealing Earth interior dynamics and surface environment change. Between Antarctica and Australia, there is a part of mid-ocean ridges of the Southeast Indian Ridge (SEIR) which has formed the ocean floor after Gondwana breakup. While the SEIR is mostly composed of hilly structured seafloor originated from magma-rich regime, anomalously deep chaotic seafloor is partly observed in the Australian-Antarctic Discordance (AAD) region. The AAD origin has been explained by weak magma supply and oceanic core complex formation as a result of cold spot, mantle convection downwelling, and/or pre-Cretaceous remnant slab (e.g., Hayes, 1976; Gurnis and Müeller, 2003; Okino et al., 2004; Liu et al., 2020). However, its evolution and migration over time is poorly understood because observational data is essentially limited. Here, we present new observational challenge to unveil seafloor spreading mode and geodynamics in the Southeast Indian Ridge. This project is based on the Science Program of Japanese Antarctic Research Expedition (JARE) and observation opportunity in the Southern Ocean provided by Japanese icebreaker *Shirase*. We aim to determine the detailed seafloor spreading history and spatio-temporal variation of topography, crust, and mantle structure from the present to about 30 million years ago. In this presentation, we introduce overview of this project including review of previous geophysical and geological studies in this region, and our preliminary results of bathymetry and magnetic anomaly observations.

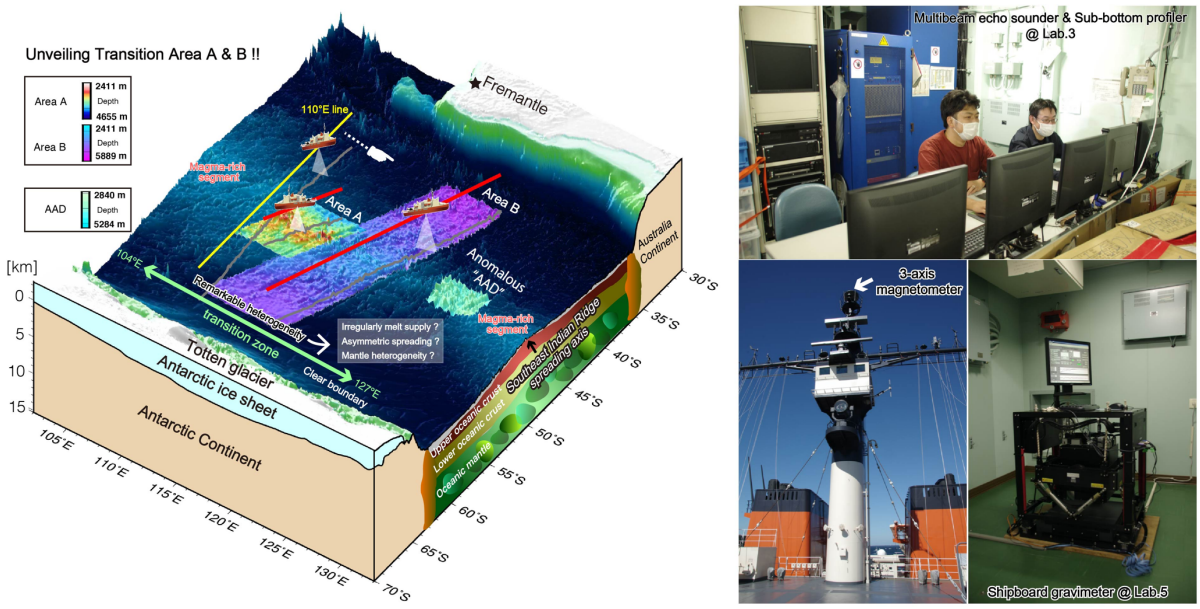

Figure. Conceptual diagram of this research

Counterclockwise and clockwise *P-T* histories recorded in a single sample? (Brattnipene, Sør Rondane Mountains, East Antarctica)

Hayato Ikeda[1], Tetsuo Kawakami[1] and Fumiko Higashino[1]
[1] *Department of Geology and Mineralogy, Graduate School of Science, Kyoto University, Japan*

The Sør Rondane Mountains (SRM) is located in the key area of Gondwana formation where the East African-Antarctic Orogen and Kuunga Orogen cross (Jacobs et al., 2003; Meert, 2003; Satish-Kumar et al., 2013). Osanai et al. (2013) divided the SRM into the NE terrane and the SW terrane, bounded by the Main Tectonic Boundary (MTB). The NE terrane is characterized by the clockwise pressure-temperature-time (*P-T-t*) path of the granulite-facies metamorphic rocks and inherited zircons older than ca. 1200 Ma, whereas the SW terrane is characterized by the counterclockwise *P-T-t* path and inherited zircons younger than ca. 1200 Ma. The Brattnipene is located in the central part of the SRM, and two counterclockwise *P-T* paths have been reported previously (Adachi et al., 2013; Baba et al., 2013). However, these studies have combined *P-T* information obtained from several different samples to construct the *P-T* paths. The aim of this study is to construct a *P-T* path using a single sample from Brattnipene. We focused on the trace element abundance of rutile and garnet and on the distribution of Al_2SiO_5 polymorphs in constraining the *P-T* path.

The sample used in this study is a Grt-Sil-Bt gneiss (TK2009120403D2) collected from the Nakayubi-ridge. The main matrix mineral assemblage is Grt+Bt+Sil+Crd+Qz+Kfs+Pl, with minor Rt+Zrn+Ap+Mnz+Po+Gr. Biotite and sillimanite are arranged parallel to the gneissosity of this sample, and quartz ribbon develops parallel to it. We divided this sample into two layers; the layer containing abundant plagioclase, K-feldspar and quartz with minor garnet (garnet A), and the layer with abundant biotite and garnet (garnet B).

The garnet A is about 1 mm in diameter and includes sillimanite. The trace element contents of garnet A determined by electron microprobe analyses were Cr~44-150 ppm, V~58-120 ppm and Nb<~84 ppm. The garnet A is replaced by the fine-grained Bt+Pl intergrowth at the rim, which is further surrounded by the coarser-grained mineral assemblage of Bt+Pl+Ky/Sil+Qz+Rt. The latter likely represents the following reaction (1) that took place during cooling:

Grt A + Kfs + H_2O or melt → Bt + Pl + Ky/Sil + Qz + Rt (1).

Adachi et al. (2013) considered that the reaction similar to (1) that lacks rutile in the product side is an evidence for the isobaric cooling. The rutile seen in the mineral assemblage replacing garnet gave trace element contents of Cr~180-460 ppm, V~630-1900 ppm, and Nb~230-8100 ppm. The Zr-in-rutile geothermometry (Tomkins et al., 2007) applied to the rutile grain gave 770 ºC at the pressure of the kyanite/sillimanite transition (0.9 GPa).

The garnet B is about 8 mm in diameter, and includes sillimanite, quartz, rutile, zircon, biotite and cordierite. The trace element contents of garnet B were Cr~31-79 ppm, V~30-100 ppm and Nb<~24 ppm. The rutile included in garnet B gave trace element contents of Cr~150-480 ppm, V~1200-2900 ppm, and Nb<~570 ppm. Because the Sil+Crd+Bt assemblage is included in garnet B, the garnet B was probably formed through the univariant reaction

Bt + Sil + Qtz = Grt + Crd + Kfs + melt (2).

Intersection between the univariant reaction curve for (2) in the KFMASH system (Wei et al., 2004) and the result of the Zr-in-rutile geothermometry (Tomkins et al.,2007) applied to the rutile inclusion in garnet B yielded 750-850 ºC and 0.5-0.7 GPa. The result of the garnet-aluminosilicate-plagioclase-quartz (GASP) geobarometry (Holdaway, 2001) applied to the mineral assemblage of matrix biotite, sillimanite, quartz and the core of garnet B was consistent with this *P-T* estimate. Some of the sillimanite grains included in the garnet B is connected to the matrix through cracks. The assemblage of Crd+Spl is developed as a thin film between the sillimanite inclusion and garnet B. This microstructure probably represents the decompression reaction:

Grt B + Sil + H_2O → Crd + Spl (3).

The Crd+Qtz symplectite is developed around the rim of garnet B. The symplectite consists of sillimanite, pyrrhotite, biotite and rutile. The symplectite probably formed during the decompression from 0.5-0.7 GPa to the pressure condition for the reaction (3) by decomposing garnet B. The Zr-in-rutile geothermometer (Tomkins et al., 2007) applied to the rutile grain (Cr~140-1500 ppm, V~490-3900 ppm, Nb~300-870 ppm) in the symplectite gave 700-800 ºC for the pressure range of 0.4-0.7 GPa, consistent with isothermal decompression *P-T* path. The Bt+Pl+Sil intergrowth cuts the symplectite.

Common to both layers, the vein-like mineral aggregate consisting of fibrous Ky+Qz±Sil±Spl±Po develops along the grain boundaries of the matrix minerals and also cuts the breakdown textures of garnets A and B described above.

In the studied sample, garnet A is richer in Cr, V, and Nb compared to garnet B. Although application of the Zr-in-rutile geothermometry (Tomkins et al., 2007) to the rutile grains yielded similar temperature conditions in most cases, systematic

difference of rutile composition in Cr, V and Nb contents was observed: (i) rutile in the coarser-grained mineral assemblage replacing garnet A is higher in Nb than other rutile grains, and (ii) rutile in the symplectite developed around garnet B is higher in Cr and V compared to the rutile enclosed in garnet B. We consider that these compositional variation of rutile with different mode of occurrence reflects different formation reactions of the rutiles. It is known that the diffusion rate of Zr in rutile is lower than that of Nb and Cr in rutile under 850 ºC (Cherniak et al., 2019). If we assume that the variation in trace element compositions in rutile grains as described above is an evidence for the preservation of their original composition, Zr concentration should be preserved as well. We consider, therefore, that the temperature conditions obtained from the Zr-in-rutile geothermometry (Tomkins et al., 2007) represent the formation temperature of each rutile grain.

The microstructures developed around garnet A indicate counterclockwise-like *P-T* history, whereas microstructures related to garnet B suggests clockwise-like *P-T* history with a decompression in the sillimanite stability field. Therefore, we observed the clockwise-like and the counterclockwise-like *P-T* evolutions from a single sample. Future work to determine the formation timings of two types of garnet is required to understand the entire *P-T-t* evolution of the Brattnipene rocks.

References

Adachi, T., Hokada, T., Osanai, Y., Nakano, N., Baba, S., Toyoshima, T., Contrasting metamorphic records and their implications for tectonic process in the central Sør Rondane Mountains, eastern Dronning Maud Land, East Antarctica, Geological Society Special Publication, 383 (1), 113-133, 2013.

Baba, S., Osanai, Y., Nakano, N., Owada, M., Hokada, T., Hiroe, K., Adachi, T., Toyoshima, T., Counterclockwise *P-T* path and isobaric cooling of metapelites form Brattnipene, Sør Rondane Mountains, East Antarctica: Implications for a tectonothermal event at the ptoro-Gondowana margin, Precambrian Research, 234, 210-228, 2013.

Cherniak, D.J., Watson E.B., Al and Si diffusion in rutile, American Mineralogist, 104, 1638-1649, 2019.

Holdaway, M.J., Recalibration of the GASP geobarometer in light of recent garnet and plagioclase activity models and versions of the garnet-biotite geothermometer, American Mineralogist, 82, 582-595, 2001.

Jacobs, J., Bauer, W., Fanning, C.M., Late Neoproterozoic/Early Paleozoic events in central Doronning Maud Land and significance for the southern extension of the East African Orogen into East Antarctica, Precambrian Research, 126, 27-53, 2003.

Meert, J.G., A synopsis of events related to the assembly of eastern Gondowana, Tectonophysics, 362, 1-40.

Osanai, Y., Nogi, Y., Baba, S., Nakano, N., Adachi, T., Hokada, T., Toyoshima, T., Owada, M., Satish-Kumar, M., Kamei, A., Kitano, I., Geologic evolution of the Sør Rondane Mountains, East Antarctica: Collision tectonics proposed based on metamorphic processes and magnetic anomalies, Precambrian Research, 234, 8-29, 2013.

Satish-Kumar, M., Hokada, T., Owada, M., Osanai, Y., Shiraishi, K., Neoproterozoic orogens amalgamating East Gondowana: Did they cross each other ?, Precambrian Research, 234, 1-7, 2013.

Tomkins, H.S., Powell, R., Ellis, D.J., The pressure dependence of the zirconium-in-rutile thermometer, Journal of Metamorphic Geology, 25, 703-713, 2007.

Wei, C.J., Powell, R., Clarke, G.L., Calculated phase equilibria for low- and medium-pressure metapelites in the KFMASH and KMnFMASH systems, Journal of Metamorphic Geology, 22, 495-508, 2004.

Monazite U-Th-Pb ages of the "unnamed nunatak (Nunatak 170224-3)" east of Forfinger Point, Western Rayner Complex, Enderby Land, East Antarctica

Tomokazu Hokada[1,2], Sotaro Baba[3], Atsushi Kamei[4] and Ippei Kitano[5,6]

[1] *National Institute of Polar Research*

[2] *Department of Polar Science, The Graduate University for Advanced Studies (SOKENDAI)*

[3] *University of the Ryukyus*

[4] *Shimane University*

[5] *Kyushu University*

[6] *Tochigi Prefectural Museum*

The Western Rayner Complex in Enderby Land attracts interest as this area being the key connection among three distinct geologic units Archaean Napier Complex to the northeast, Mesoproterozoic Rayner Complex to the southeast and the Neoproterozoic-Cambiran Lützow-Holm Complex to the west. The age of the Western Rayner Complex has been well constrained as 550-520 Ma metamorphism and ~780Ma or c.2500 Ma protoliths (Shiraishi et al., 1997, 2008). The area can be subdivided into the charnockite-dominant western part (Vechernyaya Suite; ~780 Ma?) and the mixed protolith eastern part (Forefinger Suite; c.2500 Ma?), and UHT peak metamorphic conditions and a clockwise P-T trajectory have been estimated for pelitic rocks from Forefinger Point (Harley et al., 1990; Motoyoshi et al., 1995). According to the recent SHRIMP zircon studies on the neighboring Rayner Complex (Horie et al., 2016) and the geologic field studies (JARE-58; Hokada, Baba, Kamei, Kitano), the Rayner Glacier is considered as the boundary between the ~900 Ma Rayner and the ~500 Ma Western Rayner Complexes.

We made a short (~30 minutes) field survey at a small unnamed nunatak ("Nunatak 170224-3) east of Forfinger Point at the JARE-58 (2016-2017). The nunatak area is composed of biotite gneiss, Opx-biotite gneiss and rare garnet-bearing Opx-biotite gneiss indicating granulite-facies metamorphic conditions. Monazite U-Th-Pb analyses have been conducted using electron microprobe for three samples (1702-24-3A-03, 05 and 06). Two samples (03 and 05) gave c.600-500 Ma age cluster with some older but large error (low Pb) age, with weighted average ages of 552+/-4 Ma (1702-24-3A-03) and 530+/-13 Ma (1702-24-3A-06), respectively. Some of monazite grains in 1702-24-3A-03 demonstrate core (600-550 Ma)-rim (550-500 Ma) relations. Another sample (1702-24-3A-05) includes only low-Pb monazites giving no meaningful ages.

The above lines of evidences support the c.550-530 Ma high-grade metamorphic event obtained from SHRIMP zircon studies for this area (e.g., Shiraishi et al., 1997).

References

Harley, S.L., Hensen, B.J., Heraton, J.W., Two-stage decompression in orthopyroxene-sillimanite granulites from the Forefinger Point, Enderby Land, Antarctica. Implications for the evolution of the Archaean Napier Complex. Journal of Metamorphic Geology, 8, 591-613, 1990.

Horie, K., Hokada, T., Motoyoshi, Y., Shiraishi, K., Hiroi, Y., Takehara, M., U-Pb zircon geochronology in the western part of the Rayner Complex, East Antarctica. Journal of Mineralogical and Petrological Sciences, 111, 104-117, 2016.

Motoyoshi, Y., Ishikawa, M. And Fraser, G.L., Sapphirine-bearing silica-undersaturated granulites from Forefinger Point, Enderby Land, East Antarctica: evidence for a clock-wise P-T path ! Proceedings of the NIPR Symposium on Antarctic Geosciences, 8, 121-129, 1995.

Shiraishi, K., Ellis, D.J., Fanning, C.M., Hiroi, Y., Kagami, H. and Motoyoshi, Y., Reexamination of the metamorphic and protolith ages of the Rayner complex, Antarctica: Evidence for the Cambrian (Pan-African) regional metamorphic event. In: Ricci, C.A. (ed.) The Antarctic Region: Geological Evolution and Processes. Terra Antartica, Sienna, 79–88, 1997.

Shiraishi, K., Dunkley, D.J., Hokada, T., Fanning, C.M., Kagami, H., Hamamoto, T., Geochronological constraints on the Late Proterozoic to Cambrian crustal evolution of eastern Dronning Maud Land, East Antarctica: a synthesis of SHRIMP U-Pb age and Nd model age data. In: Satish-Kumar, M. et al. (Eds.), Geodynamic Evolution of East Antarctica: A Key to the East-West Gondwana Connection. Geological Society, London, Special Publication, 308, 21-67, 2008.

Preliminary reports of U-Pb zircon age of charnockites in Aker Peaks of the Napier Complex, East Antarctica

Kenji Horie[1, 2], Mami Takehara[1], Tomokazu Hokada[1, 2] and Allen P. Nutman[3]
[1]*National Institute of Polar Research*
[2]*The Graduate University for Advanced Studies, SOKENDAI*
[3]*University of Wollongong*

The Napier Complex in East Antarctica has attracted considerable interest on account of its long Archaean crustal history from 3800 Ma to 2500Ma as well as position in Precambrian supercontinents as well as its extremely high peak metamorphic temperature (UHT: ultra-high temperature), which exceeds 1100 °C. The discovery of extremely ancient crustal material of ca. 4000Ma obtained by Pb-Pb isochron in the Fyfe Hills (Sobotovich et al., 1976) generated intense interest in the Napier Complex. Similar evidences of ancient crustal materials were reported for the Mt. Sones and Gage Ridge region (Black et al., 1986; Harley and Black, 1997). Belyatsky et al. (2011) reported Eoarchean U-Pb zircon age of 3981 ± 8 Ma from charnockites in Aker Peaks. In this study, we report preliminary geochronological and geochemical data of zircons collected from two charnockite samples of Aker Peaks.

The sample #22a is phlogopite-bearing orthopyroxene-mesoperthite-charnockite and contains zircon, monazite and rutile as accessory mineral. Phlogopite replaces orthopyroxene forming symplectites with quartz. The zircon grains contain K-feldspar, plagioclase, quartz, biotite, magnetite, apatite, monazite, and xenotime as mineral inclusions. The sample #36a is phlogopite-bearing orthopyroxene-mesoperthite-cataclastic charnockite and contains zircon as accessory mineral. Plagioclase is replaced by mesoperthite which is corroded by quartz. The zircon grains include K-feldspar, plagioclase, quartz, biotite, apatite, and monazite. The zircon garains separated from both samples were analyzed using a sensitive high-resolution ion microprobe (SHRIMP) at National Institute of Polar Research. Chemical U-Pb dating of one monazite with 100 μm width in the sample #36a was carried out by an electron probe micro analyzer (JEOL JXA-8200) at National Institute of Polar Research.

For the sample #22a, 116 spots were analyzed on 109 zircon grains and 106 spots yielded concordant data (Disc.%<10) which show age peaks at ca. 3598 Ma, 3533 Ma, and 3500 Ma. These ages are consistent with the anatexis in Oygarden Group, Kemp Land. Most zircon grains have high U content (220-4200 ppm) and then the $^{206}Pb/^{238}U$ ratios were corrected based on Williams and Hergt (2000), due to a machine-induced bias related to metamictization of grains. Th/U ratios are 0.07-0.68. On the other hand, some zircon grains in the sample #36a shows core-rim structure. 67 spots were analyzed on 37 zircon grains and 58 spots yielded concordant data (Disc.%<10). The cores and grains show age peaks at ca. 3727 Ma, 3667 Ma, 3637, 3615, 3573, and 3395 Ma. Similar age peaks are reported from charnockite and enderbite gneisses in Aker Peaks. The rims show a younger age peak at ca. 2500 Ma which is consistent with regional metamorphism in the Napier Complex. The Th/U ratios of the rims are relatively higher (0.50-1.65). 8 spots were analyzed on a monazite grain and yielded wide range ages from 2941 Ma to 2341 Ma.

References

Belyatsky, B.V., Rodionov, N.V., Antonov, A.V. and Sergeev, S.A., The 3.98–3.63 Ga zircons as indicators of major processes operating in the ancient continental crust of the East Antarctic Shield (Enderby Land). In Doklady Earth Sciences 438, 2, 770-774, 2011.

Black, L.P., Williams, I.S., Compston, W., Four zircon ages from one rock: the history of a 3930 Ma-old granulite from Mount Sones, Enderby Land, Antarctica. Contributions to Mineralogy and Petrology 94, 427–437, 1986.

Harley, S.L., Black, L.P., A revised Archaean chronology for the Napier Complex, Enderby Land, from SHRIMP ion-microprobe studies. Antarctic Science 9, 74–91, 1997.

Sobotovich, E.V., Kamenev, Y.N., Komaristy, A.A., Rudnik, V.A., The oldest rocks of Antarctica (Enderby Land). International Geology Review 18, 371–388, 1976.

Williams, I.S. and Hergt, J.M., U-Pb dating of Tasmanian dolerites: A cautionary tale of SHRIMP analysis of high-U zircon. Beyond 2000: New frontiers in isotope geoscience, 185-188, 2000.

Dependence of GIA-induced gravity change in Antarctica on viscoelastic Earth structure

Yoshiya Irie[1], Jun'ichi Okuno[1,2], Takeshige Ishiwa[1], Koichiro Doi[1,2] and Yoichi Fukuda[1]
[1]*National Institute of Polar Research*
[2]*The Graduate University for Advanced Studies, SOKENDAI*

The Antarctic ice mass loss is accelerating due to recent global warming. Changes in Antarctic ice mass have been observed as the gravity change by GRACE (Gravity Recovery and Climate Experiment) satellites. However, the gravity signal includes both the component of the ice mass change and the component of the solid Earth response to surface mass change (Glacial Isostatic Adjustment, GIA). Namely, to constrain the ice mass change from the gravity observation, viscoelastic structure of the Earth's mantle and ice history from the last deglaciation are required with sufficient accuracy.
Antarctica is characterized by lateral heterogeneity of seismic velocity structure. West Antarctica shows relatively low seismic velocities, suggesting low viscosity regions in the upper mantle. On the other hand, East Antarctica shows relatively high seismic velocities, suggesting thick lithosphere. Considering the viscoelastic structure in the Antarctic region, we evaluate the spatial and temporal patterns of the gravity field changes associated with GIA.
Results indicate that the gravity field change mainly depends on the upper mantle viscosity profile and the lithosphere thickness. In particular, the long-wavelength gravity field changes become dominant in the adoption of viscoelastic models with a low viscosity layer beneath the elastic lithosphere. The same trend is also shown in the adoption of viscoelastic models with a thick lithosphere, and there is a trade-off between the structure of the low viscosity layer and the thickness of the lithosphere. In this presentation, we will examine how this dependence of the gravity field change on the viscoelastic structure affects the GRACE estimate of Antarctic ice sheet mass change.

Monitoring and assessing the permafrost coast retreat along the Kara Sea by integrating in situ measurements

Arata Kioka[1], Vladislav S. Isaev[2], Pavel I. Kotov[2], Andrey Koshurnikov[2], Yaroslav Shevchuk[2], Takeshi Tsuji[1], Stanislav A. Ogorodov[2,3], Masakazu Fujii[4], Osip Kokin[2,5] and Michail Tsarapov[2]

[1]*Kyushu University, Japan*

[2]*Lomonosov Moscow State University, Russian Federation*

[3]*Russian Academy of Sciences, Russian Federation*

[4]*National Polar Research Institute, Japan*

[5]*N.N. Zubov State Oceanographic Institute, Russian Federation*

The Kara Sea hosts more than 25% of the total Arctic coastline. Our earlier study (Isaev et al., 2019) reveals that the Kara Sea is subject to a significant increase in the retreat rate of the permafrost coast in the recent decade, probably relating to recent climate change. However, little is understood regarding how the cliff line of the permafrost coast in the Kara Sea may have changed over time and what the climatic and environmental drivers are. This is due to that the conventional methods using satellite imagery alone are not satisfactory to understand the dynamic interplay between permafrost coast and climatic and environmental factors. A team led by Moscow State University had done continuous in-situ geological and geophysical measurements through a field campaign in the Baydaratskaya Bay of the Kara Sea for a decade. Our Russian-Japanese team aims to advance understanding the permafrost coast dynamics in the Kara Sea with the help of the intensive dataset acquired. The dataset includes the differential GPS mapping, properties of frozen soils, sediment samples, ground temperature, electromagnetic resistance tomography, drone photography, LiDAR measurements, and the estimated wave energy flux of wind-driven ocean waves along the permafrost coast. We will report the latest field survey in September 2021 and present our preliminary results, attempting to investigate the temporal and spatial changes in the permafrost coast cliff and discuss their relation to recent climate change.

References

Isaev, V.S., A.V. Koshurnikov, A. Pogorelov, R.M. Amangurov, O. Podchasov, D.O. Sergeev, S.N. Buldovich, D.M. Aleksyutina, E.A. Grishakina and A. Kioka, Cliff retreat of permafrost coast in south-west Baydaratskaya Bay, Kara Sea, during 2005–2016, Permafrost and Periglacial Processes, 30, 35-47, 2019.

Metamorphic zone mapping of the High Himalayan Crystalline nappe in Dhankuta, Eastern Nepal

Shumpei Kudo[1], Tetsuo Kawakami[1], Toru Nakajima[1,2], and Harutaka Sakai[1]
[1]*Department of Geology and Mineralogy, Graduate School of Science, Kyoto University, Kyoto 606-8502, Japan*
[2] *Tono Geoscience Center, Japan Atomic Energy Agency, Gifu 509-5102, Japan*

The Himalayan orogenic belt is mainly divided into four tectonic units, i.e., Siwalik Sequences, Lesser Himalayan Sequences (LHS), High Himalayan Crystallines (HHC) and Tethys Himalayan Sequence (THS) from the south to the north (Sakai et al., 2013). The HHC is bounded by the Main Central Thrust (MCT) to the south and the South Tibetan Detachment System (STDS) to the north (Sakai et al., 2013). Various models have been proposed to explain the formation mechanism of the HHC (Henry et al., 1997; Beaumont et al., 2001, 2004; Jamieson et al., 2004, 2006; Bollinger et al., 2006; Kohn, 2008). Previous study suggested that the HHC is a single-layered rock body exhumed from the lower crustal depth as a result of mid-crustal channel flow (Jamieson et al., 2004). On the other hand, the existence of the High Himal Thrust (HHT) within the HHC has been reported, which divides HHC into the upper and the lower HHC (Goscombe et al., 2006). Pressure-temperature-time (*P-T-t*) paths of the lower HHC and the upper HHC are reported from the Tamor-Ghuna section in far eastern Nepal (Imayama et al., 2018). Imayama et al. (2012; 2018) revealed that cordierite migmatites from the upper HHC exhumed up to shallow levels at ca. 27-25 Ma and then cooled during melt crystallization at ca. 21-17 Ma, and that kyanite-sillimanite migmatites from the lower HHC formed during partial melting at ca. 21-18 Ma and then cooled at ca. 18-16 Ma, indicating isothermal decompression, with rapid exhumation. These two different *P-T-t* paths imply the occurrence of two separate partial melting events in the upper and lower HHC (Imayama et al., 2018). Imayama et al. (2018) pointed out that it is hard to explain the exhumation of the HHC only by the channel flow model, and that in addition to the MCT and the STDS, the HHT played an important role in the exhumation of the HHC as well. However, limited number of *P-T-t* paths have been reported from limited areas of the Himalayas. Therefore, more researches on the *P-T-t* evolution of the upper and lower HHC are required in order to understand the exhumation process of the HHC.

In this study, we performed metamorphic zone mapping using metapelites collected from the north of the Dhankuta area, eastern Nepal. Our study area belongs to the lower HHC based on the location of the HHT described in Imayama et al. (2018). In the study area to the north of the MCT (cf. Kawakami et al., 2019; Sato et al., 2020), we proposed the "kyanite-in" isograd for the first time. We also mapped "sillimanite-in" and "muscovite-out" isograds, which are consistent with the locations of the "sillimanite-in" and "muscovite-out" isograds proposed by Groppo et al. (2009). We used a garnet-biotite-kyanite gneiss (sample 19111202) collected from the north of the muscovite-out isograd to determine the *P-T* evolution of the lower HHC rocks in the study area. The main matrix mineral assemblage of this sample is Grt+Bt+Ky/Sil+Kfs+Pl+Qtz. Biotite and kyanite in the matrix are arranged parallel to the gneissosity. The garnet is about 3 mm in diameter and consists of the core with abundant inclusions and the rim with a few inclusions. The core encloses kyanite, plagioclase, quartz, rutile, ilmenite and zircon, whereas the rim encloses sillimanite, plagioclase, rutile, ilmenite, zircon, and nanogranitoid inclusions. The garnet rim is partly replaced by the mineral assemblage of Bt+Sil+Qtz±Pl. From these pieces of observation, this sample is supposed to have experienced the *P-T* evolution starting from the kyanite stability field (garnet core stage) to the sillimanite stability field (garnet rim stage). The result of *P-T* estimates for these metamorphic stages using geothermobarometry will be reported in the presentation.

References

Beaumont, C., Jamieson, R.A., Nguyen, M.H. & Lee, B., Himalayan tectonics explained by extrusion of a low-viscosity crustal channel coupled to focused surface denudation. Nature, 414, 738–742, 2001

Beaumont, C., Jamieson, R.A., Nguyen, M.H. & Medvedev, S., Crustal channel flows: 1. Numerical models with applications to the tectonics of the Himalayan–Tibetan orogen. Journal of Geophysical Research, 109, B06406, 2004

Bollinger, L., Henry, P. & Avouac, J.P., Mountain building in the Nepal Himalaya: thermal and kinematic model. Earth and Planetary Science Letters, 244, 58–71, 2006.

Goscombe, B., Gray, D.& Hand, M, Crustal architecture of the Himalayan metamorphic front in eastern Nepal. Gondwana Research, 10, 232-255, 2006.

Groppo, C., Rolfo, F. & Lombardo, B, P-T evolution across the main central thrust zone (Eastern Nepal): Hidden discontinuities revealed by petrology. Journal of Petrology, 50(6), 1149–1180, 2009.

Henry, P., Le Pichon, X. & Goffé, B., Kinematic, thermal and petrological model of the Himalayas: constraints related to metamorphism within the underthrust Indian crust and topographic elevation. Tectonophysics, 273, 31–56, 1997.

Imayama, T., Takeshita, T. & Arita, K, Metamorphic P-T profile and P-T discontinuity across far-eastern Nepal Himalaya: investigation of channel flow models. Journal of Metamorphic Geology, 28, 527-549, 2010.

Imayama, T., Takeshita, T. et al, Two-stage partial melting and contrasting cooling history within the Higher Himalayan Crystalline Sequence in the far-eastern Nepal Himalaya. Lithos, 134-135, 1-22, 2012.

Imayama, T., Takeshita, T, K. YI & Fukuyama, M, Early Oligocene partial melting via biotite dehydration melting and prolonged low-pressure-low-temperature metamorphism of the upper High Himalaya Crystalline Sequence in the far east of Nepal. The Geological Society of London, Special Publications, 481, 147-173, 2018.

Jamieson, R.A., Beaumont, C., Medvedev, S. & Nguyen, M.H., Crustal channel flows: 2.Numerical models with implications for metamorphism in the Himalayan-Tibetan orogen. Journal of Geophysical Research, 109, B06407, 2004.

Jamieson, R.A., Beaumont, C., Nguyen, M.H. & Grujic, D., Provenance of the Greater Himalayan Sequence and associated rocks: predictions of channel flow models. In: Law, R.D., Searle, M.P. & Godin, L. (eds.) Channel Flow, Ductile Extrusion and Exhumation in Continental Collision Zones. Geological Society of London, Special Publications, 268, 165–182, 2006

Kawakami, T., Sakai, H., & Sato, K., Syn-metamorphic B-bearing fluid infiltrations deduced from tourmaline in the Main Central Thrust zone, Eastern Nepal Himalayas. Lithos, 348–349, 105175., 2019

Kohn, M.J., P–T–t data from Nepal support critical taper and repudiate large channel flow of the Greater Himalayan Sequence. Geological Society of America Bulletin, 120, 259–273, 2008.

Sakai, H., Iwano, H., Danhara, T., Takigami, Y., Rai, S.M., Upreti, N.N., Hirata, T., Rift-related origin of the Paleoproterozoic Kuncha Formation, and cooling history of the Kuncha nappe and Taplejung granites, eastern Nepal Lesser Himalaya: a multichronological approach. Island Arc, 22, 338-360, 2013.

Sato, K., Sakai, H., & Kawakami, T., Distribution of ductile deformation around the Main Central Thrust zone at the frontal part of nappe in southeastern Nepal Himalaya. Island Arc, 29(1), 1–9., 2020

Characteristics and evolution process of tectonic regions in the Antarctic Plate and its adjacent area based on marine geophysical data

Takeshi Matsumoto[1], and Yoshifumi Nogi[2]
[1]*University of the Ryukyus*
[2]*National Institute of Polar Research*

The Antarctic Plate including the continental region is known to be classified into 11 tectonic regions. And also, the area south of 30°S including the Antarctic Plate and its adjacent area is classified into more than 20 tectonic regions (Hayes, et al., 2009). Each tectonic region has experienced proper tectonic history and evolution process due to the continental break-up, cooling after the accretion of the oceanic crust at the mid-ocean ridges, subsidence of the seafloor due to the cooling and the oceanic sedimentaion, and transition of the oceanic plate motion by the fluctuation of the Euler pole location for past 200 milliom years. The palaeo water depth of each era in each tectonic region during this period has been reconctructed by Hayes, et al. (2009). The current study is proposed in order to clarify the uniqueness of each tectonic region, the possible interaction with adjacent tectonic regions and its transition, and finally to estimate the driving force that led the evolution of each region. This study is based on analysis of marine geophysical data (seafloor topography, gravity, geomagnetic anomaly), seafloor age, total sediment thickness, etc., which are available at NCEI (National Centres for Environmental Information, NOAA) database. Marine geophysical data acquired by R/V MIRAI and Icebreaker SHIRASE are also included for this purpose.

Since the new model of the seafloor age (Müller et al., 2016) was published after the Hayes et al. (2009) work, palaeobathymetry of 25 and 50Ma was estimated at first through the assumed age-depth relationship based on the thermal contraction model of the plates (Figure 1). Both models (Hayes et al., 2009, and this work) are consistent as for 25 Ma. However, some discrepancies take place in the Pacific Ocean area between the models: an effect of a spreading ridge off the west coast of the southernmost area of South America is found to be missing in Hayes model.

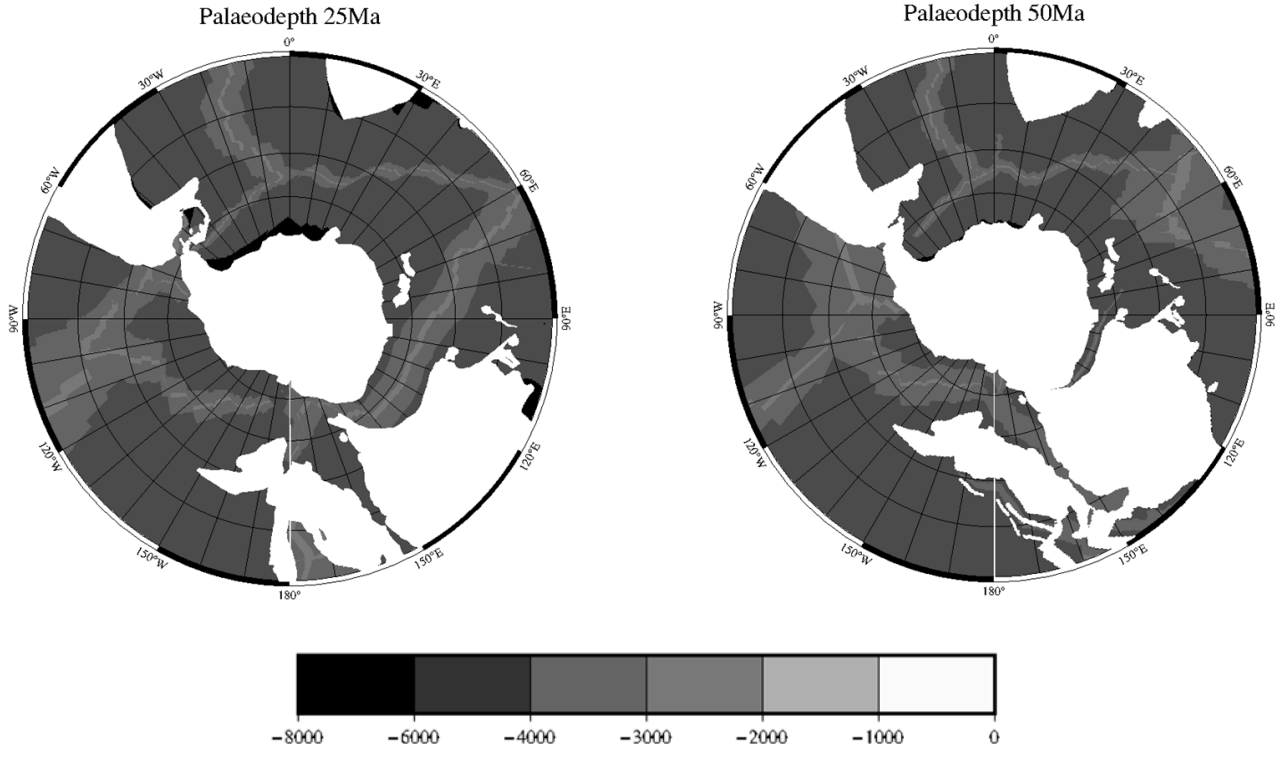

Figure 1. Re-calculated palaeotopography of the Antarctic Plate and its adjacvent area. (Left) 25Ma, (Right) 50Ma.

References

Hayes, D. E., Zhang, C., and Wessel, R. A., Modeling paleobathymetry in the southern ocean, EOS, Transactions, American Geophysical Union, 90, 165-166, 2009.

Müller, R. D., Seton, M., Zahirovic, S., Williams, S. E., Matthews, K. J., Wright, N. M., Shephard, G. E., Maloney, K. T., Barnett-Moore, N., Hosseinpour, M, Bower, D. J., and Cannon, J., Ocean basin evolution and global-scale plate reorganization events since Pangea breakup, Annu. Rev. Earth Planet. Sci., 44, 107–138, 2016.

Dependence of the Holocene rapid melting on GIA-induced vertical rate in East Antarctica

Jun'ichi Okuno[1,2], Akihisa Hattori[2], Yoshiya Irie[1], Yuichi Aoyama[1,2], Koichiro Doi[1,2] and Yoichi Fukuda[1]

[1]*National Institute of Polar Research*

[2]*The Graduate University for Advanced Studies, SOKENDAI*

Geodetic and geomorphological observations in the Antarctic coastal area generally indicate the uplift movement of the crust associated with the Antarctic Ice Sheet (AIS) change since the Last Glacial Maximum (LGM). This trend is called the glacial isostatic adjustment (GIA), the Earth's viscoelastic response due to the surface load changes. The current crustal motion, which the GNSS observation indicates, includes the elastic component due to the present-day surface mass balance of AIS in addition to the viscoelastic response. To reveal the secular crustal movement associated with the GIA, the separation of both components due to the current mass balance and last deglaciation is essential. Hattori et al. (2021) showed the GIA crustal motion using the GNSS observations in the Lützow-Holm Bay region, East Antarctica. They detected the spatial characteristics of the uplift rates, which are slightly larger for the observation site at the southern part of this area.

Recently geomorphological study in the Lützow-Holm Bay region reported that the rapid ice thinning of about 400 m for 3000 years has occurred in the early-to-mid Holocene (Kawamata et al., 2020). This melting may influence the crustal deformation through the viscoelastic response due to rapid ice load change. Therefore, we use numerical modeling to examine the GIA component due to this melting on the current crustal deformation rate. Results indicate that the viscoelastic relaxation due to the abrupt ice thinning depends significantly on the upper mantle viscosity profile. This presentation will discuss the dependence of the AIS retreat history and mantle viscosity structure on the GIA-induced crustal movement based on numerical experiments.

References

Hattori, A., et al., GNSS observations of GIA-induced crustal deformation in Lützow-Holm Bay, East Antarctica, Geophysical Research Letters, 48(13), e2021GL093479, 2021.

Kawamata, M., et al., Abrupt Holocene ice-sheet thinning along the southern Soya Coast, Lützow-Holm Bay, East Antarctica, revealed by glacial geomorphology and surface exposure dating, Quaternary Science Reviews, 247, 106540 , 2020.

Ice sheet thinning since the Last Glacial Maximum in central Dronning Maud Land, East Antarctica

Yusuke Suganuma [1,2], Heitaro Kaneda [3], Takushi Koyama [4], Takeshige Ishiwa [1], Jun'ichi Okuno [1,2], Motohiro Hirabayashi [1], and Magic DML team

[1]*National Institute of Polar Research*

[2] *Department of Polar Science, The Graduate University for Advanced Studies (SOKENDAI)*

[3] *Faculty of Science and Engineering, Chuo University*

[4]*Faculty of Education, Oita University*

The geological constraint for the past Antarctic ice sheet changes is essential to understand their climate sensitivity and to anticipate their contribution to future sea-level change. However, a large uncertainty in the past ice-sheet reconstruction, especially for East Antarctica, limits the ice sheet model validations and calibration of the satellite measurements of ice mass change via glacial isostatic adjustment (GIA) models. Here, we present a well-constrained glacial history since the Last Glacial Maximum (LGM) in Dronning Maud Land, East Antarctica, which reveals ~ 100 m thick ice sheet during the LGM rapidly retreated during early-mid Holocene (9-6 ka). This ice retreat profile allows us to validate the GIA ice load models and to estimate the freshwater discharge from this region. The climatic and GIA models suggest that the regional sea-level peaked at 12-11 ka might trigger the ice shelf collapse and following retreat in this area.

Geochemical characterization of zircons for age determination of metamorphism in Fyfe Hills of the Napier Complex, East Antarctica

Mami Takehara[1], Kenji Horie[1,2] and Tomokazu Hokada[1,2]
[1]*National Institute of Polar Research, 10-3, Midori-cho, Tachikawa-shi, Tokyo 190-8518, Japan.*
[2]*Graduate University for Advanced Studies (SOKENDAI), Japan*

Ultra-high temperature (UHT) metamorphism is critical to understanding the large-scale tectonic processes affecting the deep crust and lithosphere throughout Earth's history. The Napier Complex in East Antarctica is the location where the regional UHT metamorphism was first recognized (Dallwitz, 1968) and experienced extremely high temperatures (>1100 °C) based on the mineral assemblage of sapphirine + quartz (Harley, 2016 and reference therein). The thermal history of the Napier Complex is essential for unraveling the Earth's crustal evolution, including deep crust; however, geochronological constraints, such as the timing and duration of the metamorphic events, are still debated. Two hypotheses for the timing are proposed in previous studies: (i) the UHT metamorphism occurred no earlier than 2840 Ma and possibly from 2590 to 2550 Ma (e.g., Harley et al., 2001), (ii) it occurred from around 2500 to 2450 Ma (e.g., Carson et al., 2002).

In this study, U–Pb zircon geochronology integrated with rare earth element (REE) and oxygen isotope was applied to a garnet-bearing quartzo-feldspathic gneiss to confirm the timing of UHT metamorphism in Fyfe Hills in the western part of the Napier Complex. The quartzo-feldspathic gneiss is mainly composed of garnet + mesoperthite (ternary feldspar) + quartz, with small amounts of zircon and opaque minerals (Horie et al., 2012).

The zircons collected from the quartzo-feldspathic gneiss are observed in backscattered electron (BSE), and cathodoluminescence (CL) images obtained using the low-vacuum mode of a scanning electron microscope (JEOL JSM-5900LV) with a Gatan mini CL detector at National Institute of Polar Research, Japan (NIPR). The zircons were analyzed using a sensitive high-resolution ion microprobe (SHRIMP) at National Institute of Polar Research. After the all SHRIMP analysis, true color CL images of the grain mount were obtained using a Gatan ChromaCL2 system installed with a field emission SEM (FE-SEM; JEOL JSM-7100F) at the NIPR. The CL observation and U–Pb ages allowed us to classify the analytical domains into three types (Table 1): inherited domains (Group I), metamorphic domains (Group II), and U‑Pb system disturbed domains (Group III). The REE patterns of metamorphic domains are characterized by a weak fractionation between the middle REE and heavy REE, which reinforces the classification based on the CL observation and the U–Pb ages. The $^{207}Pb/^{206}Pb$ ages of metamorphic domains have an age peak at 2501 Ma. Therefore, the gneiss experienced high-temperature metamorphism at 2501 Ma. The $\delta^{18}O$ of zircons are homogeneous among the three groups (5.53 ± 0.11‰, 5.51 ± 0.14‰, and 5.53 ± 0.23‰), which suggests the oxygen isotope compositions in zircon were re-equilibrated after the metamorphism at ca. 2501 Ma under dry UHT conditions.

Table 1. Classification of the analytical domains in the YH05021606A zircons (modified after Takehara et al., 2020)

Classification	CL Image	U–Pb Age
Group I	oscillatory-zoning, sector-zoning, and dark CL broad zoning	older than 2501 Ma
Group II	nebulous to fir-tree zoning and bright CL broad zoning	around 2501 Ma
Group III*	(III-i) oscillatory-zoning, sector-zoning, and dark CL broad zoning (III-ii) nebulous to fir-tree zoning and bright CL broad zoning	(III-i) younger than 2501 Ma (III-ii) younger than 2450 Ma

*The domains of Group III include those of III-i and III-ii.

References

Dallwitz, W. B. Co-existing sapphirine and quartz in granulite from Enderby Land, Antarctica. Nature, 219, 476-477, 1968.

Harley, S. L., A matter of time: the importance of the duration of UHT metamorphism. Journal of Mineralogical and Petrological Sciences, 111, 50-72, 2016.

Harley, S. L., P. D. Kinny, I. Snape, and L. P. Black, Zircon chemistry and the definition of events in Archaean granulite terrains. Paper presented at the Fourth International Archaean Symposium, Extended Abstract Volume, 2001

Carson, C. J., Ague, J. J., and Coath, C. D. U–Pb geochronology from Tonagh Island, East Antarctica: implications for the timing of ultra-high temperature metamorphism of the Napier Complex. Precambrian Research, 116, 237-263, 2002.

Horie, K., T. Hokada, Y. Hiroi, Y. Motoyoshi, and K. Shiraishi, Contrasting Archaean crustal records in western part of the Napier Complex, East Antarctica: New constraints from SHRIMP geochronology. Gondwana Research, 21, 829-837, 2012.
Takehara M, K. Horie, and T. Hokada, Geochemical Characterization of Zircon in Fyfe Hills of the Napier Complex, East Antarctica. Minerals, 10, 943, 2020.

Ancient earthquakes and E-W compressional stress field recorded by brittle faults and pseudotachylytes from southwestern Skarvsnes in the Lützow-Holm Complex, East Antarctica

Tsuyoshi Toyoshima[1], Ippei Kitano[2,3], Masahiro Ishikawa[4], Takuma Katori[1,5] and Tomokazu Hokada[6]

[1] *Niigata University*

[2] *Kyushu University*

[3] *Tochigi Prefectural Museum*

[4] *Yokohama National University*

[5] *Fossa Magna Museum*

[6] *National Institute of Polar Research*

Pseudotachylytes were found north of Lake Naga (Naga-ike) and Lake Kikuno (Kikuno-ike) of southwestern Skarvsnes in the Lützow-Holm Bay region. They are called Naga-ike PST and Kikuno-ike PST, respectively. The Naga-ike PST is associated with an ENE-WSW trending main fault (Naga-ike Fault) that steeply dips north and a length of more than 300 m. The Kikuno-ike PST is associated with an NNW-SSE trending main fault (Kikuno-ike Fault) that moderately dips east and a length of more than 100 m. The Naga-ike and Kikuno-ike Faults, which cut gneissose structures of surrounding rocks, consist of pseudotachylytes, cataclasites, brittle fractures, echelon faults and spray structures. The Naga-ike and Kikuno-ike Faults are dextral strike-slip faults and have occasionally produced ancient earthquakes and formation of pseudotachylytes. Part of pseudotachylytes and cataclasites of the Naga-ike and Kikuno-ike Faults have a reddish color. The field evidence suggests that the Naga-ike and Kikuno-ike Faults and PSTs were formed under oxidizing conditions at shallow depths. The Kikuno-ike Fault is associated with a larger amount of cataclasite than the Nagaike Fault. The Nagaike Fault is associated with a larger number of tension fractures (T veins) filled with pseudotachylyte veins than the Kikuno-ike Fault. Most pseudotachylyte veins along the Kikuno-ike Fault are Y veins.

The Kikuno-ike Fault and PST appear to be cut and displaced by the Naga-ike Fault. The Kikuno-ike and Naga-ike Faults and PSTs appear to have resulted from different earthquakes under different tectonics. The trend and shear sense of the Naga-ike Fault are the same as those of D4 dextral ENE-WSW-trending faults reported by Yoshida (1978). The D4 faults are widely distributed in the central region of the Soya Coast and were formed under E-W compressional stress field without metamorphic and igneous effects (Yoshida, 1978). Therefore, it is concluded that the Naga-ike Fault and PST resulted from a regional E-W compressional stress and may have been related to the formation of complex geological structures of the central region of the Soya Coast.

C-O-H fluid was present during the garnet-forming partial melting in the Aoyama area, Ryoke metamorphic belt, SW Japan

Natsumi Yoshimoto[1] and Tetsuo Kawakami[1]

[1]*Department of Geology and Mineralogy, Graduate School of Science, Kyoto University, Kyoto 606-8502, Japan*

The crustal rocks have low porosity, and contain small amount of H_2O (Sawyer et al., 2013). Therefore, fluid-absent dehydration melting has long been considered as the dominant partial melting process in the crust. Incongruent melting above the wet solidus generates peritectic mineral(s) and melt. Melt inclusions in peritectic minerals are widely considered as the textural evidence of dehydration melting (e.g., Cesare et al., 2009). Recently, however, melt inclusions and COH fluid inclusions have been reported from the same domain of a peritectic garnet in migmatites (e.g., Carvalho et al., 2019). This microstructure indicates that the COH fluid phase coexisted during the garnet-forming incongruent melting. The presence of fluid phase has a great influence on the partial melting process of the crustal rocks such as melting temperature, melt chemistry, and melt viscosity (Weinberg and Hasalová, 2015). Investigating melting process in other crustal section will help us understand whether the partial melting in the presence of the COH fluid phase is a common phenomenon in the crust. Therefore, we investigated in detail the partial melting process of the migmatitic rocks from the Aoyama area, Ryoke metamorphic belt, SW Japan.

In the Aoyama area, the dominant rock facies changes from pelitic and psammitic schists in the northern part to metatexite and diatexite migmatites in the southern part (Kawakami, 2001). The migmatite is mostly metatexite near the schist/migmatite boundary, whereas diatexite becomes common in the southern part of the migmatite dominant area (Kawakami, 2001). The Aoyama area has been divided into one contact metamorphic zone produced by post-tectonic granite intrusion and two regional metamorphic zones. The Sil-Kfs zone, in which Ms+Qtz is unstable and Sil+Kfs is stable, is located in the schist-dominant, northern area. The Grt-Crd zone, in which Grt+Crd+Bt+Kfs±Sil is stable, is located to the south of the Sil-Kfs zone (Kawakami, 2001). Migmatites dominate in the Grt-Crd zone except for the northwestern part (Kawakami et al., 2013). The pressure-temperature (*P-T*) condition of peak metamorphism in the Aoyama area is previously estimated using the garnet-biotite geothermometers and the garnet-aluminosilicate-plagioclase-quartz (GASP) geobarometers to be 3.0-4.0 kbar, 615-670 ℃ in the Sil-Kfs zone, and 4.5-6.0 kbar, 650-800 ℃ in the Grt-Crd zone (Kawakami, 2001). Melt inclusions are reported as inclusions in metamorphic zircon rim showing ca. 92-90 Ma from the Aoyama area (Kawakami et al., 2013; 2019). However, details of the prograde partial melting process, including the presence or absence of fluid phases, have not been investigated in detail.

Sample B81 is a massive pelitic diatexite without foliation collected from the metatexite dominant area of the Grt-Crd zone (Kawakami, 1999MS). Metatexite and diatexite are in contact with each other in the outcrop. The sample mainly consists of quartz, plagioclase, biotite and garnet. The garnet exhibits xenomorphic shape and Bt+Pl replaces the rim of garnet. The garnet has almost homogeneous major element composition except for the rim in contact with secondary biotite. The garnet is divided into the inner core, the outer core, the mantle, the inner rim, and the outer rim based on the discontinuous chemical zoning in P. The inner core and the outer core have relatively high Y concentration compared to other domains, and the outer core encloses prograde xenotime inclusions. Sillimanite needles are included in the mantle and the inner rim. K-feldspar and muscovite inclusions are present in the vicinity of the sillimanite inclusions in the inner rim. The outer rim contains abundant ilmenite inclusions and rare euhedral plagioclase. Fluid inclusions are ubiquitous in garnet, and are composed of fluid and solid phases. Most of the fluid phases are CH_4, with rare CO_2+CH_4. Solid phase is composed of chlorite, clay minerals, and siderite. Variable proportion of CH_4 and CO_2 in the COH fluid inclusions accompanied by solid phase has been considered as the product of the post-entrapment reaction between the COH fluid and host garnet (e.g. Carvalho et al., 2019). We consider that the solid phases were produced as the secondary daughter minerals through the post-entrapment reaction.

Sample Y07C1 is a pelitic diatexite collected from the diatexite dominant area of the Grt-Crd zone (Kawakami, 1999MS). It mainly consists of quartz, plagioclase, biotite and garnet. The garnet exhibits xenomorphic shape and Bt+Pl replaces the rim of garnet. The garnet has almost homogeneous major element composition except for the rim in contact with secondary biotite. The garnet is divided into the core, the mantle, and the rim based on discontinuous chemical zoning in Y. The core encloses abundant ilmenite inclusions, rare euhedral plagioclase, and fluid inclusions. Fluid inclusions are composed of fluid and solid phases. The fluid phase is CH_4 or CH_4+CO_2. The solid phase is confirmed to be carbonate mineral(s).

Sample Y39A is a pelitic diatexite collected from the diatexite dominant area of the Grt-Crd zone (Kawakami, 1999MS). It mainly consists of quartz, plagioclase, biotite, garnet and K-feldspar. The garnet is 5 mm in diameter and shows poikiloblastic texture. The garnet is divided into the core rich in ilmenite inclusions and the rim with minor ilmenite, abundant zircon, minor rutile grains, rare euhedral plagioclase, and fluid inclusions. Plagioclase, quartz, and biotite inclusions are ubiquitous in the garnet. Fluid inclusions are composed of fluid and solid phases. The fluid phase is CH_4±CO_2, and the solid phase is carbonate

mineral(s). The rutile inclusion in the garnet rim is ~10 μm in diameter. The Zr-in-rutile geothermometer (Tomkins et al., 2007) applied to the rutile inclusion yielded preliminary temperature estimate of 717 ℃ at 5 kbar, which is consistent with the previous temperature estimate for the Grt-Crd zone.

Based on above observation, the prograde garnet growth and partial melting in sample B81 is summarized as follows. Relatively high Y concentration and presence of prograde xenotime inclusion in the garnet core implies that the garnet core grew at the similar temperature condition as a diatexite sample studied by Kawakami et al. (2019), approximately at 530-570 ℃ (Kawakami et al., 2019). Muscovite, K-feldspar, sillimanite inclusions, and fluid inclusions in the inner rim of garnet indicates that muscovite breakdown reaction Ms + Qtz + fluid → Sil + Kfs + (H_2O or melt) occurred in the presence of COH fluid. Euhedral plagioclase enclosed in the outer rim of garnet is a microstructural evidence of partial melting (e.g., Hiroi et al., 1995). Abundant ilmenite inclusions in the garnet outer rim can be explained by the incongruent melting of Ti-bearing biotite and formation of ilmenite that probably took place in the presence of the COH fluid during the prograde metamorphism, such as Bt + Sil + Qtz + fluid → Grt + Kfs + Ilm + melt. Samples Y07C1 and Y39A have abundant ilmenite inclusions in the garnet core. Garnet in both samples encloses euhedral plagioclase inclusions, which coexist with the COH fluid inclusions. This suggests that incongruent melting of biotite took place in the presence of the COH fluid and formed the garnet core. Therefore, pieces of observation from samples Y07C1 and Y39A are consistent with the garnet growth. We consider that the prograde partial melting scenario constructed from sample B81is widely applicable to the pelitic migmatites in the Aoyama area. We confirmed for the first time in this study that incongruent melting of Ti-bearing biotite took place in the presence of COH fluid phase in the pelitic migmatites of the Aoyama area.

References

Carvalho, B. B., Bartoli, O., Ferri, F., Cesare, B., Ferrero, S., Remusat, L., Capizzi, L. S., & Poli, S. (2019). Anatexis and fluid regime of the deep continental crust: New clues from melt and fluid inclusions in metapelitic migmatites from Ivrea Zone (NW Italy). Journal of Metamorphic Geology, 37(7), 951–975. https://doi.org/10.1111/jmg.12463

Cesare, B., Ferrero, S., Salvioli-Mariani, E., Pedron, D., & Cavallo, A. (2009). "Nanogranite" and glassy inclusions: The anatectic melt in migmatites and granulites. Geology, 37(7), 627–630. https://doi.org/10.1130/G25759A.1

Hiroi, Y., Motoyoshi, Y., Shiraishi, K., & Ellis, D. J. (1995). Proc. NIPR Symp. Antarct. Geosci., 8, 107-120, 1995. 107–120.

Kawakami, T. (1999). Migmatites in the Aoyama district, Ryoke metamorphic belt ⋯the relationship between tourmaline distribution and rock facies Unpublished Master's Thesis submitted to Kyoto University.

Kawakami, T. (2001). Tourmaline breakdown in the migmatite zone of the Ryoke metamorphic belt, SW Japan. Journal of Metamorphic Geology, 19(1), 61–75. https://doi.org/10.1046/j.0263-4929.2000.00298.x

Kawakami, T., Yamaguchi, I., Miyake, A., Shibata, T., Maki, K., Yokoyama, T. D., & Hirata, T. (2013). Behavior of zircon in the upper-amphibolite to granulite facies schist/migmatite transition, Ryoke metamorphic belt, SW Japan: Constraints from the melt inclusions in zircon. Contributions to Mineralogy and Petrology, 165(3), 575–591. https://doi.org/10.1007/s00410-012-0824-7

Kawakami, T., Horie, K., Hokada, T., Hattori, K., & Hirata, T. (2019). Disequilibrium REE compositions of garnet and zircon in migmatites reflecting different growth timings during single metamorphism (Aoyama area, Ryoke belt, Japan). Lithos, 338–339, 189–203. https://doi.org/10.1016/j.lithos.2019.04.021

Sawyer, E. W., Cesare, B., & Brown, M. (2011). When the continental crust melts. Elements, 7, 229-234. https://doi.org/10.2113/gselements.7.4.229

Tomkins, H. S., Powell, R., & Ellis, D. J. (2007). The pressure dependence of the zirconium-in-rutile thermometer. Journal of Metamorphic Geology, 25(6), 703–713. https://doi.org/10.1111/j.1525-1314.2007.00724.x

Weinberg, R. F., & Hasalová, P. (2015). Water-fluxed melting of the continental crust: A review. Lithos, 212–215, 158–188. https://doi.org/10.1016/j.lithos.2014.08.021